(12)

FINAL REPORT

ONR SBIR #N90-003

Fine Scale Measurements of Microwave Backscatter from the Ocean Surface

1990

Submitted by

James B. Mead

Quadrant Engineering
55 Cherry Lane
Amherst, MA 01002

Table of Contents

Statement "A", contract number is N00014-90-C-0108 per telecon Dr. Frank Herr. Office of Naval Research/code 1121. VHG 12/11/90

Chapter I

Introduction

A. Motivation for Fine-Scale Ocean Surface Radar Measurements

Radar backscatter from the ocean surface is a topic of great interest to the Navy owing to the important role of radars in many shipborne and airborne systems. Numerous experimental and theoretical research programs have been supported by the Office of Naval Research and other Federal agencies, in an effort to better understand how electromagnetic scatter is related to the hydrodynamics of the ocean surface. Knowledge of how the Normalized Radar Cross Section, σ°, of the ocean surface changes with sea state has been obtained [1,2] and this information has been used to remotely sense ocean surface winds and waves [3,4]. The growing use of Synthetic Aperture Radars (SARs) increases the need for better understanding of electromagnetic scattering by the ocean surface so the Navy can achieve the full benefits of high-resolution imaging of the ocean surface.

Interest in microwave imaging of the ocean surface is exemplified by the MARSEN and SAXON experiments, and the substantial amount of theoretical modeling [5–14] that has taken place for more than a decade. An excellent summary of the status of theory up to 1985 is provided by Hasselmann, et al. [15], but there are still some issues that remain in contention that need to be tested by future experiments. Experiments are ongoing at wave tanks at the Naval Research Laboratories (NRL) and other laboratory sites, on research towers such as the Federal Republic of Germany's North Sea Tower during SAXON-FPN, and over the open ocean using aircraft such as the Surface Wave Dynamics Experiment (SWADE) planned for 1990–91.

Wave tank, tower, and aircraft measurements offer advantages and disadvantages to the experimenter. Wave tank conditions are controllable but it is difficult to simulate a wide range of ocean conditions or to obtain radar measurements that exclude all effects of the wave tank on the measurements. At the other extreme, scattering measurements made from aircraft measure realistic surface conditions but accurate surface truth is difficult to obtain. Tower measurements represent a compromise where the surface wave conditions — although limited — are fairly realistic and accurate ground truth measurements are available.

The ONR-sponsored TOWARD and SAXON-CLT tower experiments have been useful because a variety of mechanical sensors were used to measure the ocean wave spectrum, atmospheric and water temperatures, surface wind direction, etc., concurrently with radar measurements. Furthermore, SAR images of the ocean surface were obtained during the experiment, which can be compared with the ground truth and tower radar measurements. To date, little has been done to analyze SAR images in terms of the tower measurements:

almost all data reduction has thus far been aimed at understanding the relationship between data from the tower sensors. Although this represents a necessary first step, the importance of tower data to SAR imaging remains unknown at this time.

The best spatial resolution of SAR images of the ocean surface during TOWARD, SAXON-CLT, and (the planned) SAXON-FPN experiments are (will be) approximately 1 m $\times$ 1 m, which is greater than the spatial resolution of the tower radars. Typically, the antennas of the tower radars have small apertures with the result that their footprints on the ocean surface are larger than SAR pixels. This will limit the use of data from most — but not all — tower based radars. It would be very desirable to have a tower-based radar with resolution similar to that of a SAR.

B. Functional Description of Focused-Array Radar

High resolution radars typically require large physical or synthetic apertures to achieve fine spatial resolution coupled with wide radiated bandwidths for fine range resolution. These criteria are met in a variety of ways in modern radars systems, depending on system and program constraints, such as radar velocity, limitations on the physical size of the antenna, and cost. Perhaps the most sophisticated of the real aperture radars are active phased arrays, in which each element of the array, often numbering in the thousands, is backed by a transmit/receive module, capable of transmitting and receiving precisely phased microwave radiation. Such systems are capable of rapid electronic steering of the radiated beam in both azimuth and elevation and thus can track many targets simultaneously without moving the antenna. Such a system would be prohibitively expensive for ocean surface imaging, and would, in fact, be more sophisticated than necessary.

Because the ocean surface is nearly planar it is not necessary to have narrow beams in both azimuth and elevation. A narrow azimuth beamwidth, coupled with fine range resolution, can be used to locate the pixel in space. Thus, the antenna must be large only in one dimension (the horizontal plane) which greatly reduces its complexity and cost. Furthermore, if the range of velocities of the target is small it is not necessary that the elements of the array be illuminated simultaneously, rather, they may be excited sequentially. Once all elements of the array have been sampled, an image may be formed by processing algorithms similar to those used by Synthetic Aperture Radar (SAR) imaging systems. In fact, the array may be thought of as a synthetic aperture system, except instead of moving a single antenna through space at a constant velocity, antenna "velocity" is synthesized by varying the sampling time between adjacent elements in the array. Thus, such a system may be thought of as a hybrid of synthetic and real aperture techniques.

A conceptual diagram of the antenna is shown in Figure 1.1. The antenna is shown mounted on an ocean observation tower, such as the Chesapeake Tower [16], placing the antenna at a height of approximately 28 m. Other possible configurations could include a blimp mounted antenna with fixed position or ship mounted antenna on a stabilized

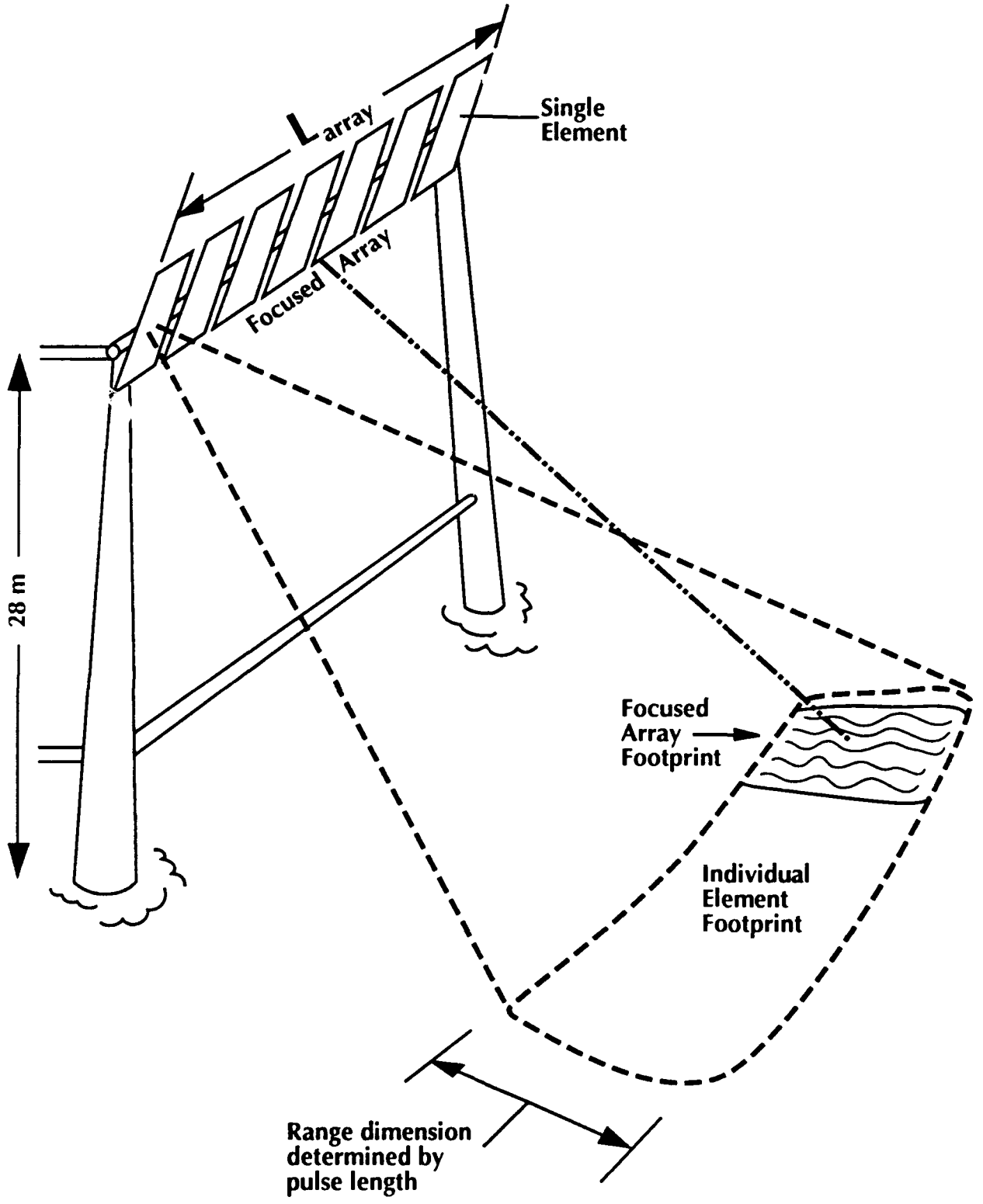

Figure 1.1 Focused array mounted on ocean observation platform.

platform. Each individual element in the array has a broad beamwidth (20°–30°), while the array beamwidth is relatively narrow (< .5°). Unlike normal antennas which are focused at infinity, this array may be focused to any point in space by adding appropriate phase shifts to the sampled element voltages in software.

C. Summary of Report

This body of this report summarized research performed by Quadrant Engineering, Inc. under the Phase I SBIR contract "Fine–Scale Measurements of Microwave Backscatter from the Ocean Surface". Chapter II provides background information necessary to understand the operation of the radar, including a review of the radar range equation for short pulse radars and basic sampled array theory. A detailed description of the proposed X- Band focused array system is given in chapter III. Also included are predictions of signal–to–noise ratio as a function of range, and a discussion of the data acquisition system.

Chapter IV describes a processing algorithm, developed by Quadrant Engineering which has been used to simulate the response of the proposed system to a hypothetical tilt modulated ocean surface. This software has been used as a design tool in evaluating the proposed radar, but may also serve as the core of a processing algorithm used in processing actual data should an actual system be deployed. We present simulations of the response of the radar to point targets at several signal–to–noise levels.

Chapter V discusses how such a system might be used in applications of interest to oceanographers and others interested in interactions of electromagnetic radiation with the ocean surface. One obvious application of this system is to study backscatter as a function of ocean sea state. In particular, the ability to degrade azimuthal and range resolution in software will allow the dependence of backscattering statistics on pixel size to be studied. The issue of what mechanism causes waves to appear in SAR generated ocean images may also be studied experimentally with this radar. We show that the proposed tower based system may be used to simulate typical R/v ratios (R = range, v = synthetic velocity) which are thought to affect spatial resolution in SAR images.

Another application discussed in chapter V is creation of a "motion picture" of the instantaneous backscattering of the ocean surface. Such moving pictures may be useful in detecting ship wakes or observing periodic behavior, such as propagation of long gravity waves with wavelengths exceeding the swath dimensions. We conclude Chapter V with a brief discussion of possible technological spin–offs of such a system.

A study of image degradation due to finite synthetic velocities is included in appendix A.

Chapter II

System Considerations

In the following sections we present background material necessary to understand the functioning of the radar system. This includes a review of the radar range equation for planar surfaces, and a summary of the important parameters in focused array design. This is followed by a presentation of a recommended design centered at 10.2 GHz, and concludes with a discussion of the data acquisition system.

A. Radar Range Equation for Planar Surface

Prediction of signal-to-noise ratio (SNR) as a function of range is a crucial step in any radar design problem. The radar range equation has been presented by many authors [17-19], and is usually cast in a form which is germane both to the radar system and to the type of problem being considered. The pulse-length limited radar range equation, given in terms of SNR is:

$$SNR = \frac{P_t L_{sys} G^2 \lambda_0^2 c\tau \phi_{az} \sigma^\circ}{128 kTBF\pi^3 R^3 \sin\psi} \tag{2.1}$$

where:

P_t = transmit power (peak)

L_{sys} = system losses (two-way)

G = antenna gain

λ_0 = wavelength

$c\tau$ = pulselength

ϕ_{az} = azimuthal beamwidth

σ° = normalized radar cross section

kTB = noise power

F = system noise figure

R = range to target

ψ = incidence angle (0° = nadir)

The pulse-length limited equation has been used because the dimensions of the illuminated footprint are limited in the range direction by the radiated pulse width, not by the elevation beamwidth. Equation 2.1 will be used in Chapter III along with models of ocean backscattering coefficient to evaluate the performance of the system. In Chapter IV we use (2.1) in conjunction with the imaging software to study the ability of the radar to accurately reproduce ocean surface images.

B. Focused Array Theory

While normal antenna arrays have their radiation focused at infinity, it is possible to focus an array to any point in space by employing an appropriate phase taper across the aperture. Figure 2.1 shows the geometry of the problem. In order to focus the antenna to a point in the near field, phase delay, β_i, in the i^{th} element feed line is adjusted such that $\beta_i - \phi_i$ = constant. According to [20], focal-distance to array-length ratios (R/L_{array}) as small as 2 have radiation patterns which differ from the far field pattern by 2 dB or less at all points within the principle plane, and are nearly identical within the main beam. Thus, provided the array is properly phased, the beamwidth of the antenna may be approximated by λ/L_{array}. Focusing the array has negligible effect beyond ranges of $2(L_{\text{array}})^2/\lambda$, i.e. in the far field [21].

1. *Sampled Array*

A subtle difference exists between real arrays, in which all elements are excited simultaneously, and a sampled array, in which the elements are sampled sequentially, such as in a SAR. Consider the two-way pattern of a real array in a radar scattering configuration. The scattered voltage present at any element represents the sum of all fields generated by the element itself plus all other elements within the array. In contrast, in a sampled array, the response at any one element is due only to the scattered fields generated by that element. Mensa [22] has derived expressions for both the real and sampled array array patterns. Figure 2.2 compares the far field patterns of sampled and focused arrays. For a given aperture illumination, the sampled array can be seen to have a narrower main beam and higher sidelobes than the associated real aperture antenna. For a uniform amplitude illumination, the sampled array two-way beamwidth is given by $0.6\lambda/L_{\text{array}}$. The two-way first sidelobe level equals 13.6 dB. By comparison, the real array beam width is given by $0.88\lambda/L_{\text{array}}$, with a first sidelobe level of 27.2 dB.

One advantage of the sampled array is that the complex voltage measured at each element may be stored and processed with any desired amplitude and phase taper. By using an appropriate amplitude taper, a reasonable trade off between beamwidth and sidelobe level may be achieved. We have found that applying an amplitude taper of $\cos^{1.8}(\pi x/L_{\text{array}})$ achieves a 30 dB first sidelobe level, with beamwidth given by λ/L_{array} (two-way). The azimuthal footprint width at range R is equal to $R\lambda/L_{\text{array}}$. If a footprint width of 1 meter is required at a range of 200 meters, $L_{\text{array}} = 200\lambda$ (12 meters at 6 GHz; 6.7 meters at 10.0 GHz).

Focusing the array to a particular point in space is achieved by using a phase taper which is quadratic in nature. For example, to focus the beam at a range R, a phase taper

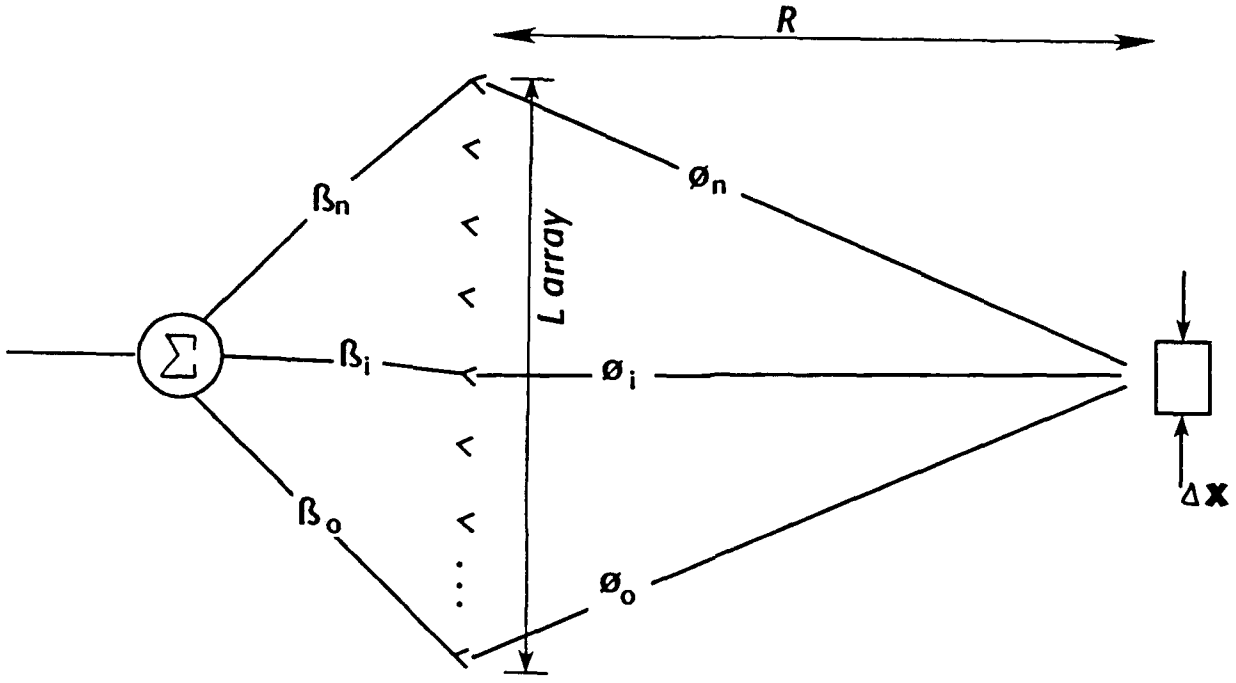

SELECT $ß_i$ SUCH THAT:

$$ß_i + ø_i = \text{CONSTANT}$$

$$\Delta x \approx \frac{R\ \lambda}{L\ array}$$

Figure 2.1 Employing phase compensation to focus array of elements to a point.

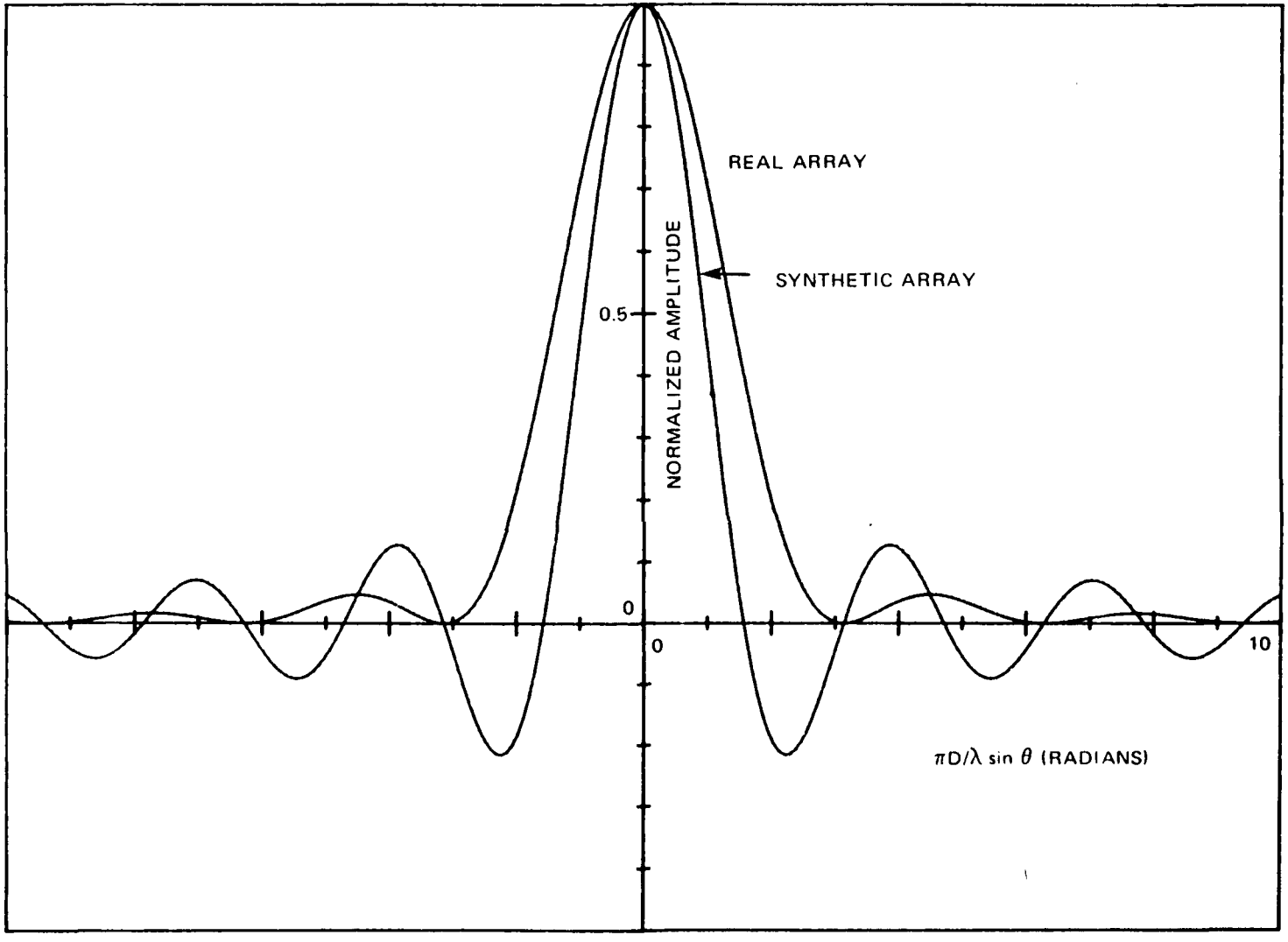

Figure 2.2 Two-way responses of real and synthetic array [22].

given by

$$\beta_i = \frac{4\pi x_i^2}{\lambda R} \tag{2.2}$$

where

$\beta_i = i^{th}$ element phase shift

$x_i =$ position of the i^{th} element

will provide a broadside beam. In Chapter IV we describe an algorithm which computes the proper phase correction at any point in space; such algorithms may operate on a single set of sampled voltages to create a two dimensional image of the object plane (plane of the surface being imaged).

2. *Grating Lobe Suppression Using Pattern Multiplication*

Proper array design usually requires that the elements spacing and phase taper be selected to place a single main beam at the desired radiation angle, while suppressing radiation as much as possible at all other angles. A lobe other than the desired main beam which is equal in amplitude to the main beam is called a *grating lobe*. In a conventional array, a grating lobe occurs when the elements comprising the array are spaced greater than $\lambda/2$ apart. For a sampled array, the grating lobe criteria is twice as stringent, i.e. $S_{\text{element}} < \lambda/4$. Many antenna arrays comprised of discrete elements avoid the problem of grating lobes by employing individual elements designed to suppress radiation in the direction of the grating lobe. The principle of pattern multiplication dictates that the net pattern of the antenna array is the product of the array radiation pattern (array factor) and the element pattern (element factor) [23]. The criteria to avoid grating lobes in a sampled array when each discrete element in the array is comprised of an antenna of width D_{element} is:

$$S_{\text{element}} = D_{\text{element}}/2 \, . \tag{2.3}$$

This is the well known SAR result [24]. However, in the sampled focused array such a criteria requires that the elements physically overlap. There are at least two solutions to this problem. One method requires creating a subarray out of pairs of elements as shown in Figure 2.3. The elements are excited by a switching network which combines adjacent elements in pairs to make two element subarrays. Note that subarray 1 overlaps with subarray 2 such that criteria (2.3) is met. Although such a scheme would work, it requires a rather complex switching network, with N additional power dividers, N additional $SP2T$ switches and $3N$ additional precision cables.

A more sensible solution to the grating lobe suppression problem, is to employ an antenna element whose projected physical aperture is considerable smaller than its effective aperture as a radiator. End fire antenna elements have such a property. The effective aperture, $D_{\text{effective}}$, of an end fire element is given by

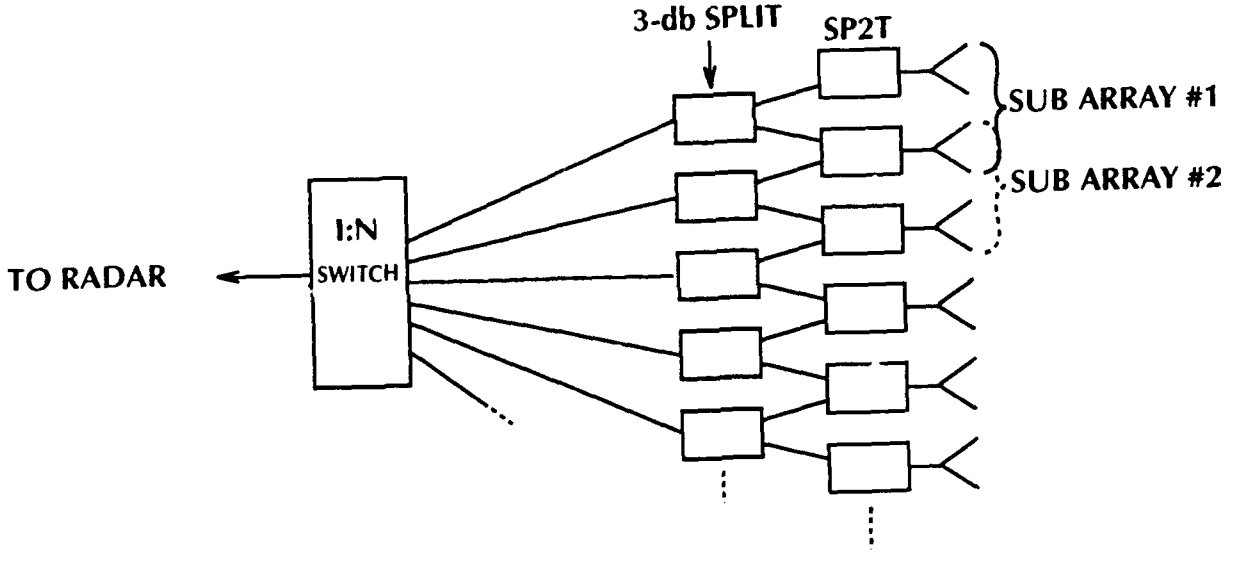

Figure 2.3 Pairing of adjacent elements to create subarray.

$$D_{\text{effective}} = \sqrt{\lambda L_{\text{element}}} \tag{2.4}$$

where L_{element} is the length of the element parallel to the direction of propagation. The 3-dB beamwidth (one-way) of such elements is approximately

$$\phi_{\text{end-fire}} = \sqrt{\lambda / L_{\text{element}}} \quad \text{radians} \tag{2.5}$$

A practical upper limit on L_{element} is about eight wavelengths. This results in $D_{\text{effective}} = 2.8\lambda$, and $\phi_{\text{end-fire}} = .35$ radians. Now the criteria (2.3) may be met with an element spacing $S_{\text{element}} = 1.4\lambda$, using elements which do not physically overlap, and with no additional complication to the switching network.

3. *Exponentially Tapered Slot Antenna Elements*

The focused array uses end-fire elements as described above. After considering several options, we settled on an end-fire element known as the Exponentially Tapered Slot Antenna (ETSA), shown in Figure 2.4. The antennas are made by etching a tapered slot in a conducting ground plane supported by a low dielectric constant plastic substrate. The ground plane may be gold plated to prevent corrosion. These antennas are broadband, low loss, straight forward to design and are inexpensive to reproduce. Quadrant Engineering plans to hire a consultant from the University of Massachusetts Antenna Laboratory to direct the design, testing and fabrication of these antenna elements.

C. Degradation due to Nonplanar Surface

In creating an image of the ocean surface, it is necessary to assume that the surface is planar, as we have no a priori knowledge of the surface height. It is conceivable that under certain conditions large deviations from the planar assumption could cause a error in focusing. A first order analysis shows that as long as the wave amplitude, ζ_c meets the criteria:

$$\zeta_c \ll \sqrt{2R\ \delta R} \tag{2.6}$$

where δR is the range resolution of the radar, and R is the range to the target. For wave amplitudes less than 3 m, ranges greater than 50 m, and δR = 1-2 m, there will be no significant distortion to the image resulting from the planar assumption.

X-BAND PROTOTYPE

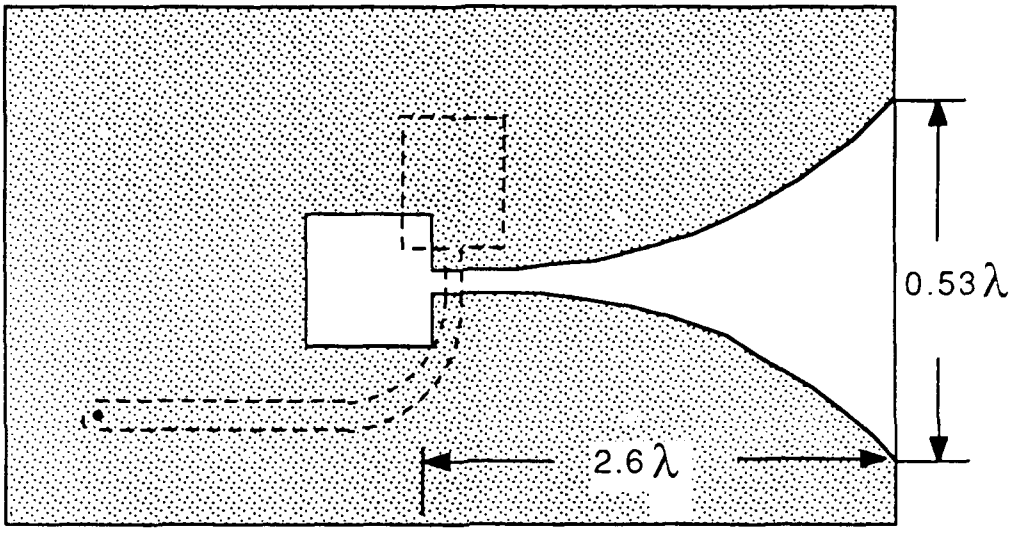

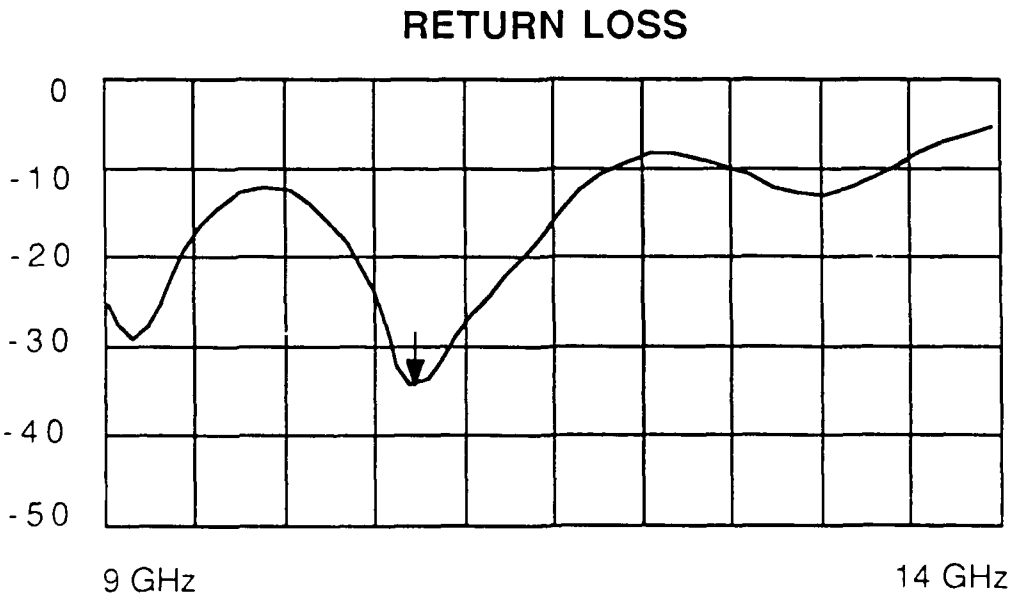

Figure 2.4 Exponentially tapered slot antenna.

Chapter III

Proposed X-band System

One of the primary goals of this Phase I study was to design a first class system for making focused array measurements within the cost constraints of a Phase II SBIR. In this chapter we detail such a design. Discussions with the remote sensing community indicated that either C-band (4 to 8 GHz) or X-band (8 to 12 GHz) would be a good choice for operating frequency. By considering tradeoffs between resolution and antenna size as well as availability of commercial components we decided that operation near 10 GHz would provided the best compromise.

Figure 3.1 is a block diagram showing the major components of the X-band system. We have selected an operating frequency of 10.2 GHz (λ = 2.94 cm). The components include a conventional short pulse radar, a 1:128 switching network to sequentially select antenna elements, the antenna, a fast data acquisition system with a fast cache memory, and a control/display computer console. These subsystems will be described in detail below.

A. Antenna and Switching Network

The antenna assembly consists of a frame which will support the individual ETSA radiating elements, individual coaxial feed lines for all elements, and a switching network mounted to the frame as shown in Figure 3.2. The entire antenna assembly will be attached to an elevation-over-azimuth positioner capable of rapidly scanning the array to any sector within the field of view of the tower. The antenna will be enclosed in a radome to protect the elements from a potentially corrosive environment. Due to the potential for high cross-polarization from the ETSA elements we may elect to etch a linear polarizing grid on the face of the radome.

1. *Array Trade-offs*

In order to simplify the switching network design we have elected to confine the number of elements to a power of 2. Given that $S_{\text{element}} = 1.4\lambda$, Table 2.1 gives antenna size, beamwidth and footprint size at 200 m range for several values of N. We have picked $N = 128$ as a reasonable compromise between spatial resolution and antenna size. A 5.2 m long antenna (17 feet) is not unreasonably long to control using a medium size antenna positioner. The possibility of scanning such an antenna to yield large area coverage makes it more attractive than the fixed position design originally conceived.

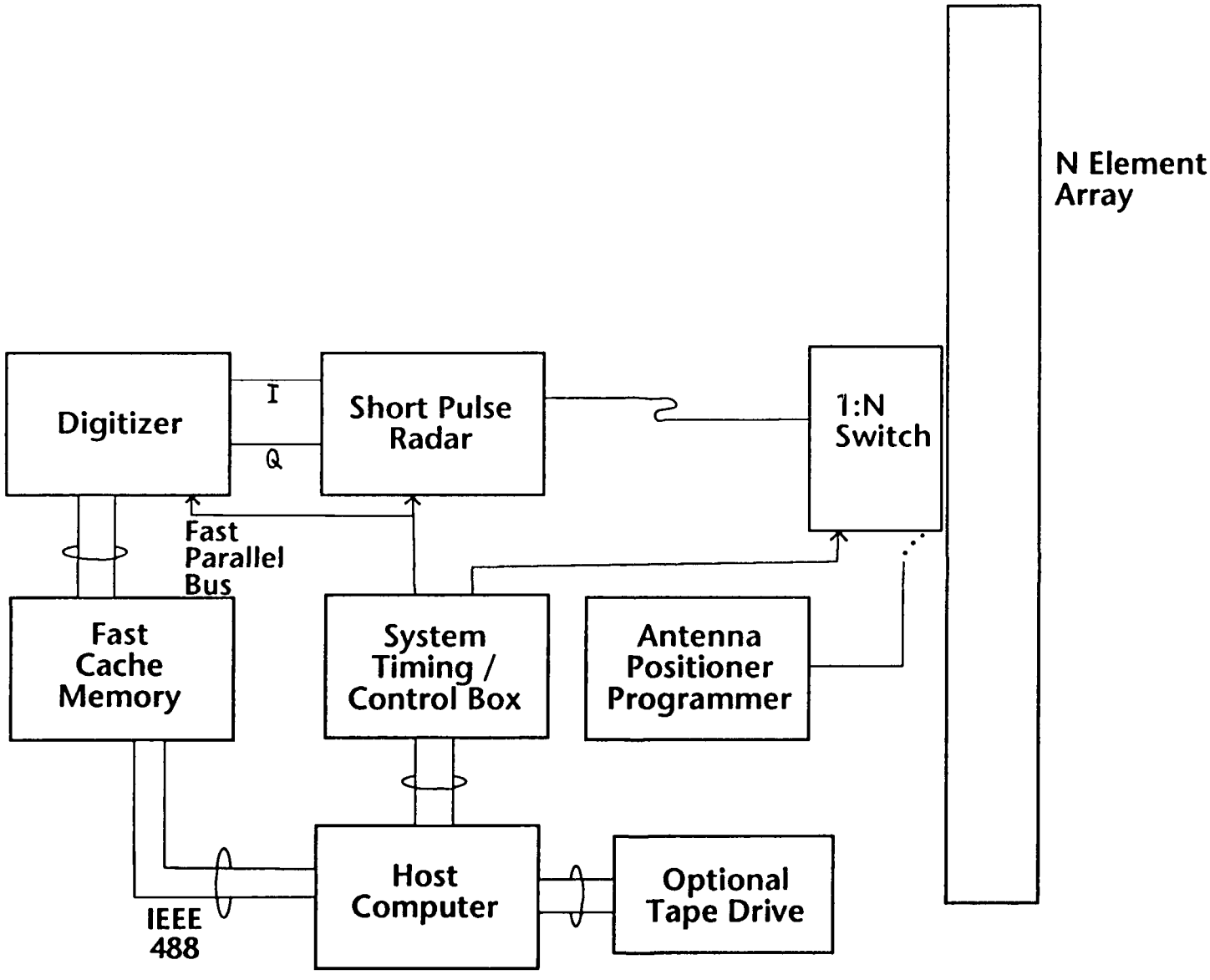

Figure 3.1 Block diagram of focused array radar system.

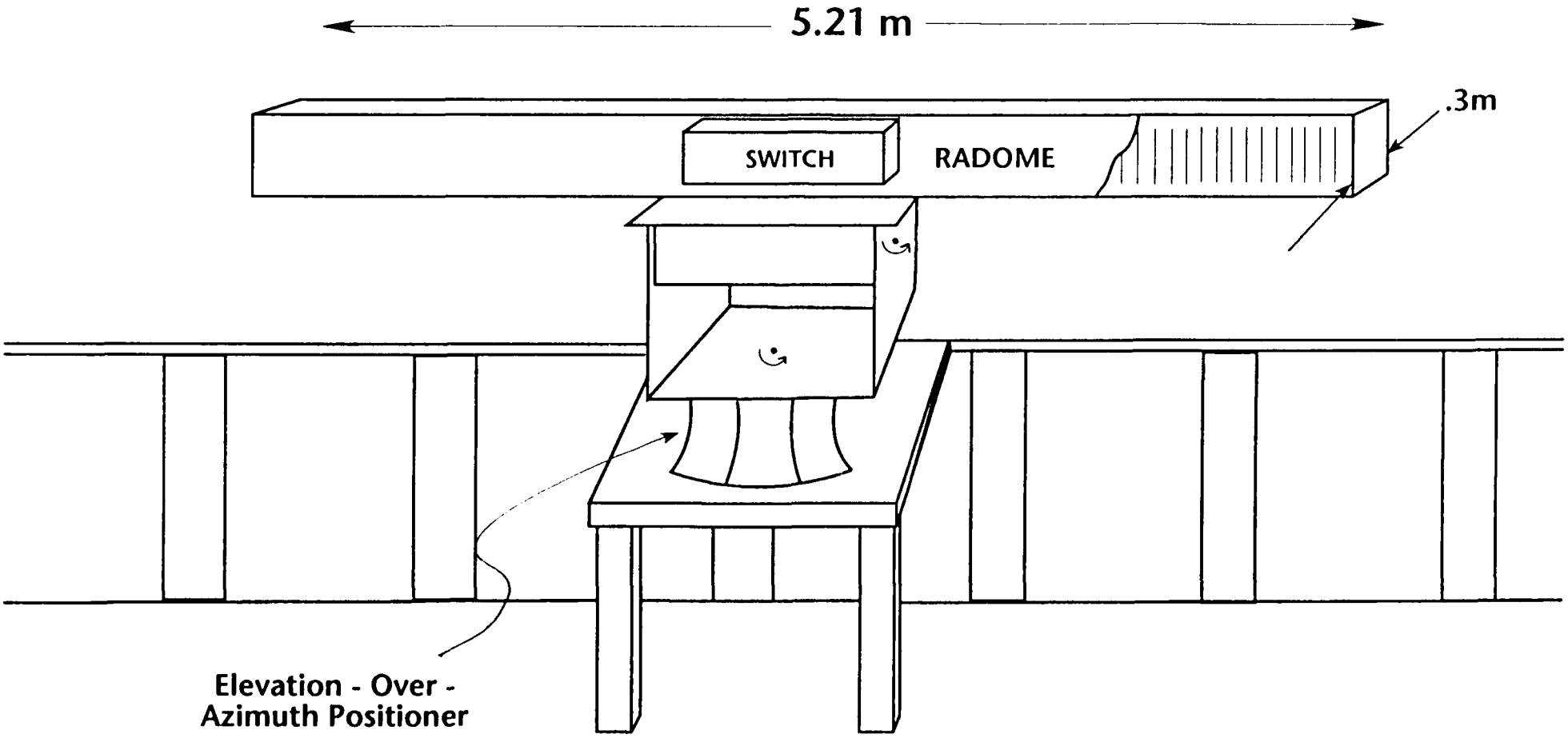

Figure 3.2 X-band focused array.

Table 2.1
X–Band Focused Array Trade–Offs

Number of Elements	Length of Array [m]	6 dB, Two–Way Beamwidth [Degrees]	Azimuth Resolution at 200 m Range [m]
32	1.27	1.33	4.51
64	2.58	0.66	2.26
128	5.21	0.32	1.13
256	10.46	0.16	0.56

2. *Switching Network*

The switching network will consist of a tree of SP2T and SP8T switches as shown in Figure 3.3. This network will be mounted directly to the antenna frame, thus allowing semi-rigid cabling between the switching network and the antenna elements. The switches have an insertion loss of approximately 2.5 dB each, thus the total insertion loss for the network will be approximately 8 dB. This loss will be encountered both in transmission and reception, thus these losses will have a significant impact on system SNR. Fortunately, the system has sufficient power and sensitivity to overcome such losses while maintaining adequate signal-to-noise performance. A single low-loss flexible coaxial cable will be used to connect the radar to the switching network.

B. Short Pulse Radar Design

In order to achieve range resolution comparable with the azimuthal resolution of the radar, it is necessary to use a very short pulse radar. For example, range resolution of 1 m will require a 6.6 nS pulse. Because it is difficult to transmit large amounts of energy in so short a pulse, it is often desirable to use some sort of pulse expansion/compression technique to increase the signal energy while conserving fine range resolution. One drawback of a pulse compression radar is that the minimum range of the radar is constrained by the length of the expanded pulse. For example, a pulse compression ratio of 100 on a 5 nS pulse results in a minimum range of 75 m. However, under certain circumstances, it would be desirable to use the proposed radar to make observations at closer ranges.

To get around these conflicting requirements, we have designed a radar using a hybrid of a real short pulse radar and a pulse compression radar. A block diagram of the proposed system is shown in Figure 3.4. For short ranges, the expander/compressor circuitry will be switched out of the circuit, allowing a minimum range of 10.4 m (constrained only by the ability to focus the antenna). As will be shown below, the system will have sufficient SNR to image the ocean surface in this mode to at least 100 m range. Beyond ranges of 100 m, the expander/compressor circuitry may be switched in, increasing the SNR by approximately 16 dB. Using commercially available expansion/compression networks, we are able to produce a compressed pulse width of about 12 nS, yielding a range resolution of 1.8 m. This will yield a square pixel at ranges near 200 m.

Due to the inherently high loss of the switching network, the radar will require a substantial amplifier in the output stage of the transmitter. Solid state X-band amplifiers capable of greater than 10 W output are currently available from several manufacturers. We have selected a unit capable of delivering 20 W peak power. Table 2.2 lists the salient features of the X-band radar system. These parameters are used to compute SNR performance below.

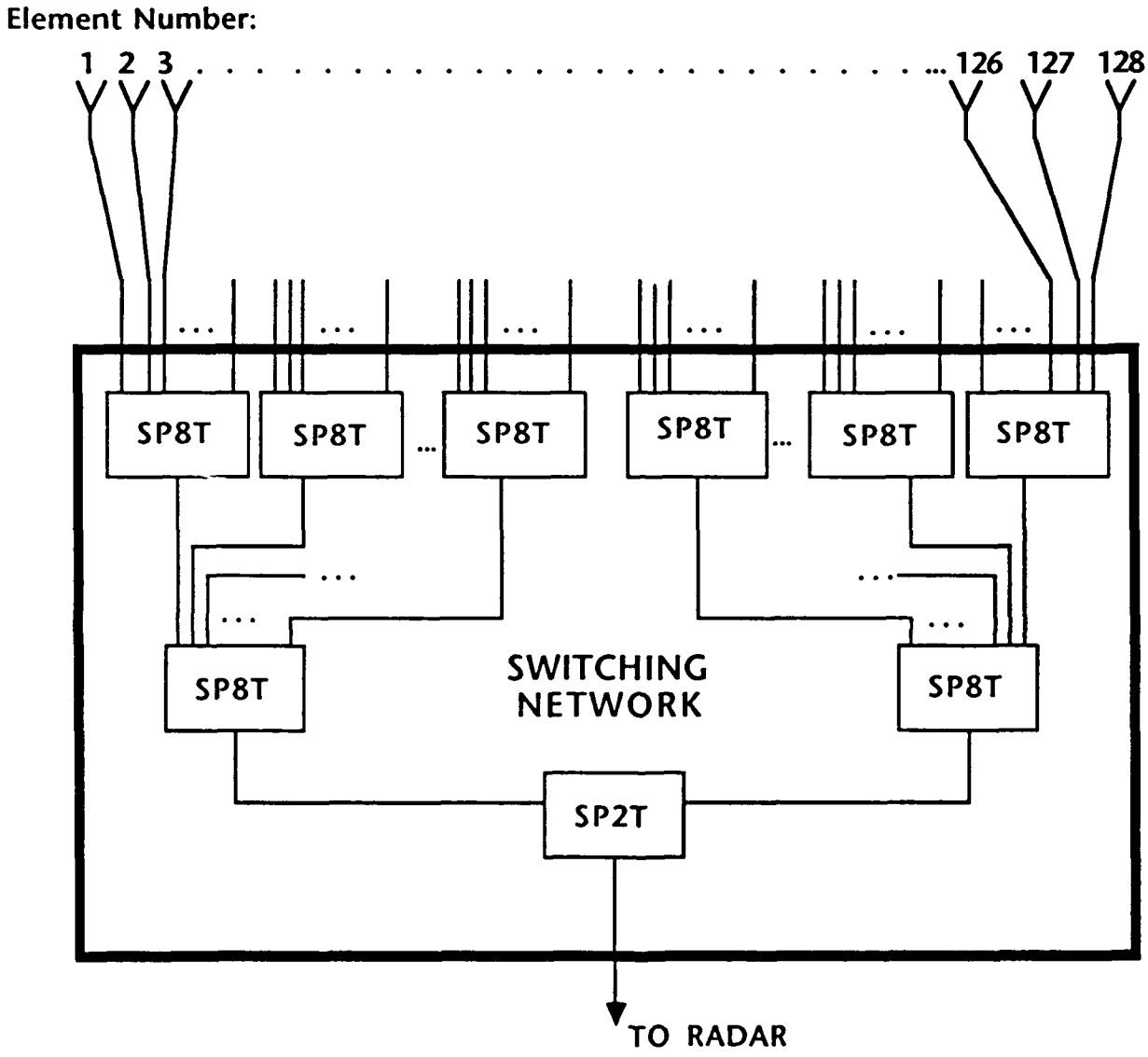

Figure 3.3 1:128 switching network.

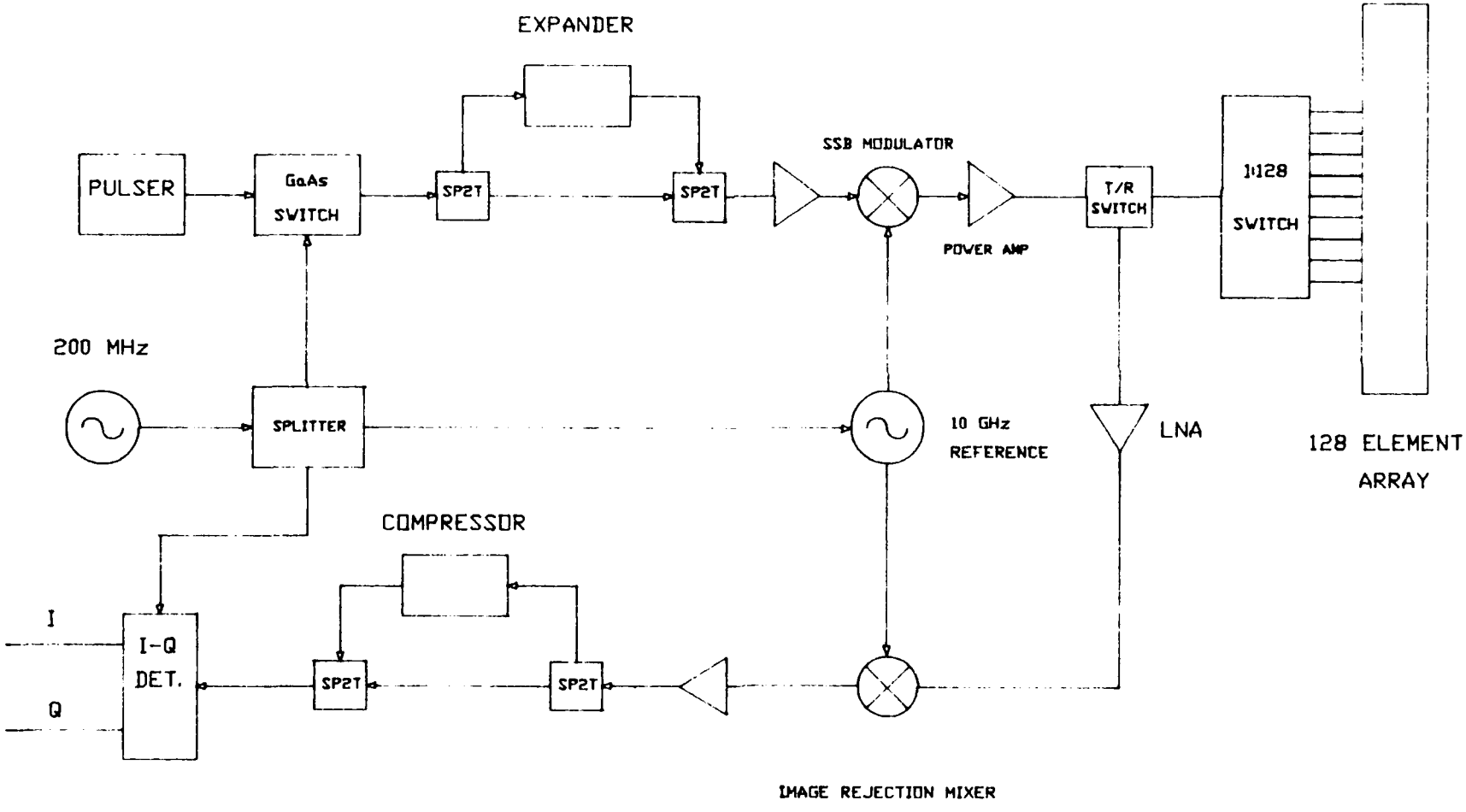

Figure 3.4 Block diagram of short pulse radar.

Table 2.2
Specifications of X–Band Focused Array Radar

Frequency:	10.2 GHz
Transmit Power	20 W (peak)
Antenna Gain:	36.3 dB
Number of Elements:	128
Azimuth Beamwidth:	0.32°
Elevation Beamwidth:	20°
Pulse Length:	6–12 nS
Range Resolution:	0.9–1.8 m
Noise Bandwidth:	200 MHz
System Noise Figure:	4 dB
System Dynamic Range:	60 dB

C. Signal–to–Noise Evaluation

The parameters given in Table 2.2 may be used in conjunction with (2.1) to compute SNR versus incidence angle or range. Given a tower height, h, range, R, is related to incidence angle, ψ, through

$$\cos\psi = h/R \tag{2.7}$$

A model of ocean surface scattering based on measurements at C–band was used to compute σ° [25]. According to [26], σ° is roughly independent of frequency in the range of angles between 20° –80°, and increases with frequency near grazing and near nadir, thus this model should be adequate for X–band simulations.

A plot of SNR as a function of range is given in Figure 3.5, assuming a tower height of 28 m for upwind and crosswind conditions. The SNR is seen to be greater than 14 dB for ranges up to 100 m without pulse compression, and greater than 13 dB for ranges up to 400 m with pulse compression.

When predicting the average SNR of a system, it is sufficient to consider the normalized radar cross section, σ°, which is a measure of the average scattering behavior of a spatially distributed target (two dimensional). However, fluctuating targets such as the ocean surface display radar backscatter which is a function of time, and thus a knowledge of the distribution of scattering amplitudes is necessary in studying system performance. We have modelled scattering from the ocean surface as having a Rayleigh distribution of amplitudes, due to the simplicity of the mathematical formulation. While Rayleigh statistics are probably insufficient in probability of detection and false alarm studies, we believe they are sufficiently representative of ocean surface scattering to model the effects of fading on SNR and image production.

For a Rayleigh fading process, 95 percent of the signal falls within 13 dB of the mean, thus an average SNR of greater than 13 dB will be necessary for good reproduction of the statistics associated with the a Rayleigh fading target. We have targeted 20 dB as a reasonable value for mean SNR, which should be sufficient to accurately measure the statistics of all but the weakest few percent of the scattered amplitude distribution. According to Figure 3.5, SNR should exceed 20 dB for all wind directions for ranges up to 200 m.

D. Data Acquisition Requirements

Data acquisition system (DAS) requirements are driven by several factors. These include number of channels, digitizing rate, video bandwidth, dynamic range, record length, data transfer rate (throughput) and data storage volume. The number of channels is relatively small, as the radar has only two outputs, I and Q. The bandwidth of these signals will be approximately 200 MHz, (5 nS rise time), which is a fairly stringent requirement

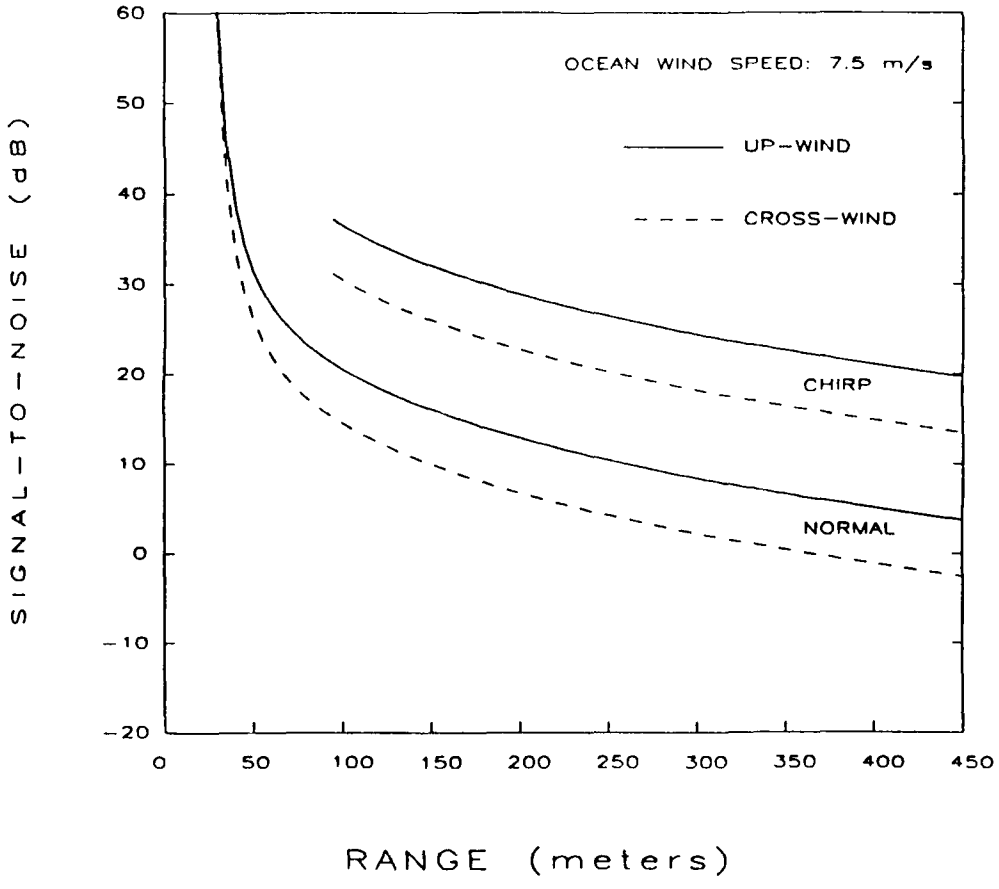

Figure 3.5 SNR versus range for upwind and cross-wind conditions, with and without pulse compression.

for a digitizing system. Current Analog-to-Digital converter (ADC) technology has advanced to the stage where several hundred MHz of video bandwidth is possible with 12 bit accuracy. A 12 bit ADC will provide a dynamic range of 72 dB which should be sufficient for accurate phase and amplitude measurements without using an automatic gain control.

Several commercial data acquisition systems are currently on the market which appear to be able to meet the requirements of the proposed radar system. One which looks particularly attractive is manufactured by Analytek, a division of Tektronix, known as the system 2000. We have been negotiating with Analytek for several months and have settled on a design whose specifications are given in Table 2.3. The series 2000 high speed digitizing cards have sufficient on board memory to store 64 range gates for each of 128 elements. For a pulse repetition frequency (PRF) of 5.62 microseconds it will take .72 mS to sample all the elements, which will fill the buffers with 16 K words. It then takes 4.37 mS to clock out the data from the digitizing cards, thus a complete image containing 64 range gates may be sampled and stored every .72+4.37 = 5.1 mS. We estimate that the ocean surface decorrelation time is on the order of 10 mS. Thus we could over sample such a process by a factor of 2. Should we desire to over sample by a greater factor, we could reduce the number of range gates.

The data throughput rate when running at the maximum rate will be 3.14 Mwords/s which is too high to store directly to the host computer. A solution to the problem is to use a fast data cache, such as the Storage Concepts system 61, which uses a series of hard discs running in parallel. The system 61 can support a sustained throughput rate of 15 Mwords/s which will be more than adequate for our uses, and has a total data volume of 800 Mwords. Presumably we could measure the ocean surface for several hundred seconds at the full data rate then download 800 Mwords to high volume tapes for later processing, freeing up the 800 M/word cache for further measurements.

Table 2.3
Specifications of Analytek Data Acquisition System

Digitizing Rate:	500 M Samples/S
Word Length:	12 bits
Video Bandwidth:	>300 MHz
Internal Storage:	8 kWords/Channel (I and Q)
Throughput Rate:	3.14 MWords/sec

Chapter IV

System Simulation Software

An important task included in the Phase I study was the development of a software package to simulate measurements of the ocean surface using a sampled focused array radar. The resulting programs have proven useful not only as an aid to designing the radar and antenna, but have provided insight into some subtle aspects of focused array behavior. This chapter includes a qualitative discussion of two software packages, FARSIM and FSIMSNR. FARSIM (Focused Array Radar SIMulator) simulates the response of the focused array to a variety of user defined surfaces, the output of which may be used to create a simulated image. FSIMSNR (Focused array radar SIMulator Signal-to-Noise Ratio) is used to compute the signal to noise ratio as a function of range for a general pulsed radar system used to observe an ocean surface.

A. Focused Array Radar Simulator Software

A flow chart of the focused array radar simulator software package, FARSIM, written in FORTRAN, is shown in Figure 4.1. The major functional blocks are SYSDEF which defines the radar system; OBJDEF which defines object plane (target) reflectivity distribution; RESPONSE which computes the complex voltage measured by each element of the radar in response to the target; and FOCUS which combines the response of all element using the proper phase and amplitude taper to focus the antenna to a given pixel in the object plane. The output of the program includes the power distribution of the image generated by the radar along with the original object plane distribution for comparison.

Figure 4.2 is a listing of the data file used to define the system parameters. Options include frequency of operation, antenna parameters, height of antenna, range resolution, etc. Figure 4.3 shows the data file used to specify the target. Options include 11 different object plane amplitude distributions (Impulse, Uniform, Rayleigh, etc.), number of pixels, iterations, SNR options, etc. The number of iterations is set to one for fixed targets, while it is often desirable to average several images when observing fading targets (options 10 and 11) to reduce image speckle [27]. Option 11 models the ocean surface radar cross-section as having Rayleigh fading statistics, with the mean value tilt modulated by a single wavelength ocean wave specified by the user. While this is an idealized model of the ocean surface it should suffice to test the ability of the focused array to extract meaningful information from a random surface.

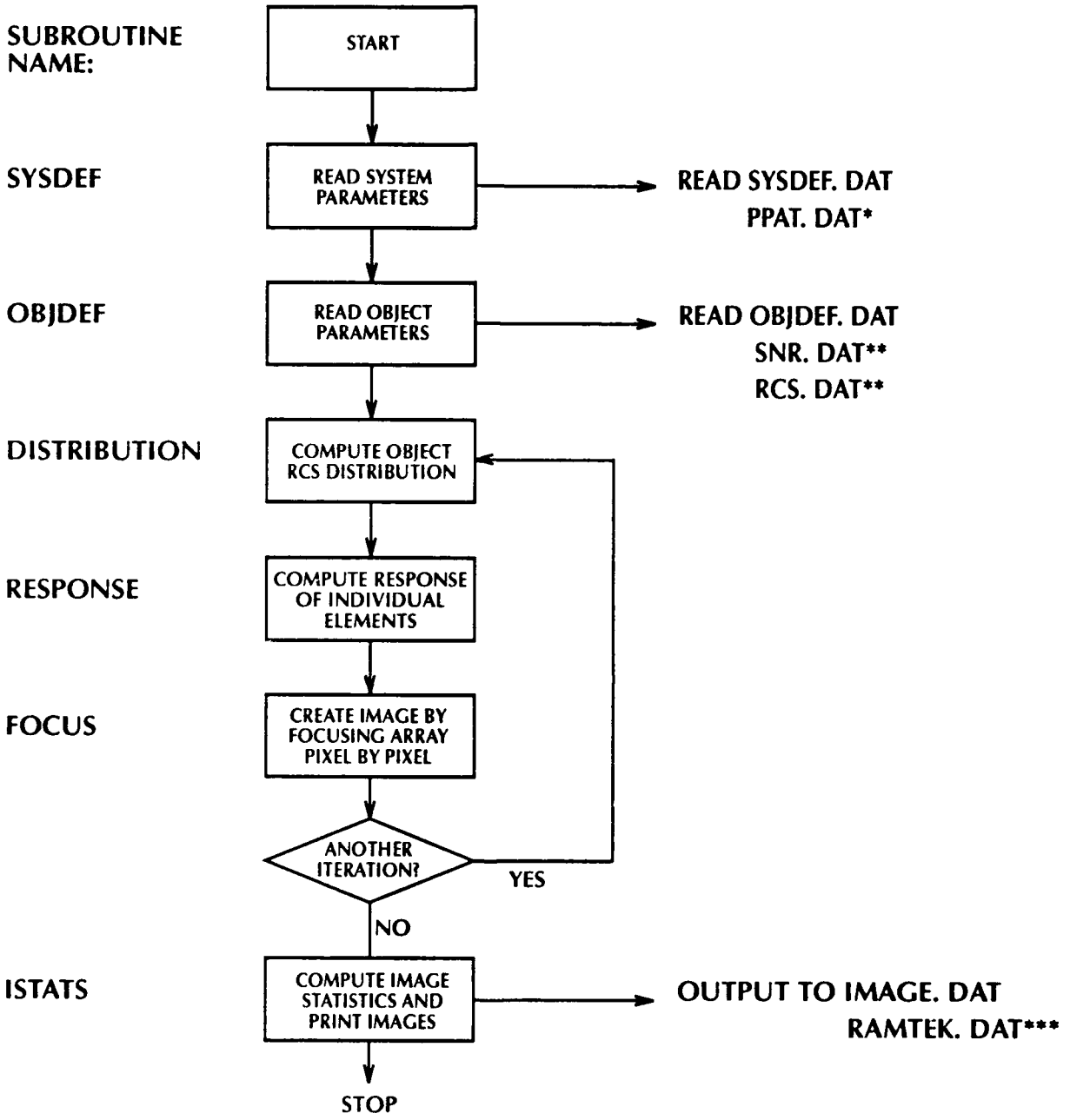

* ELEMENT FACTOR INFO (OPTIONAL)

** OPTIONAL DATA FOR OCEAN WAVE IMAGES

***OPTIONAL FOR CREATING COLOR IMAGE

Figure 4.1 Flow chart of focused array radar simulation software.

THIS DATA FILE CONTAINS INFORMATION ON THE ANTENNA AND PULSE CHARACTERISTICS OF THE FOCUSED ARRAY RADAR SYSTEM

OPERATING FREQUENCY, FGHZ, IN GHZ 10.2

NUMBER OF ELEMENTS IN THE ARRAY: NEL 128

SPACING BETWEEN ELEMENTS, DARRAY, IN METERS .0411

COSINE TAPER EXPONENT, TAPER 1.8

RANGE RESOLUTION, RRES, IN METERS 1.8

HEIGHT OF ARRAY, ZARRAY, IN METERS 28.0

ELEMENT FACTOR: NFACTOR. 0=NONE; 1=FIND ELEMENT FACTOR IN PPAT.DAT; 1

CHIRP FLAG: ICHIRP=0 FOR NO CHIRP; ICHIRP=1 FOR CHIRP BEYOND 90 METERS, 1

Figure 4.2 Listing of data file used to determine system parameters.

THIS FILE CONTAINS TARGET (OBJECT) PARAMETERS FOR USE BY THE FOCUSED ARRAY SOFTWARE

TYPE OF TARGET: 1= IMPULSE; 2 =UNIFORM RCS; 3=STEP; 4=RAMP;

CHECKER BOARD; 6=SINUSOID IN X; 7=SINUSOID IN Y;

RAYLEIGH FADING; 9=INVERSE IMPULSE; 10=SINE MODULATED RAY.

11=10 WITH NON-PLANAR SURFACE

NTYPE: 11

FIXED (0) OR RANDOM PHASE(1): IPHASE 0

NUMBER OF ITERATIONS 1

Y COORDINATE OF NEAREST PIXEL, YNEAR, IN METERS 125.0

PIXEL SPACING, PSPACE, IN METERS 1.0

NUMBER OF PIXELS IN Y (PERPENDICULAR TO ARRAY), NPEL 50

NUMBER OF PIXELS IN X (PARALLEL TO ARRAY), NPAZ 50

INTEGER SEEDS FOR RALEIGH DISTRIBUTION, I1/I2 53223 554531

PIXEL LOCATION FOR IMPULSE, AZIMUTH, IK 25

PIXEL LOCATION FOR IMPULSE, ELEVATION, IJ 25

SIGNAL TO NOISE FLAG: ISNR=0 FOR INFINITE SNR; =1 FOR STORED SNR; =2 FOR FIXED 1

IF ISNR=2 USE THE SNR IN dB, GIVEN BELOW (INDEP. OF RANGE), SNR_DB: 0.0

WAVE AMPLITUDE OF WAVE MODULATING RAYLEIGH SURFACE, WAVE_AMP IN METERS: 1.0

WAVELENGTH OF WAVE MODULATING RAYLEIGH SURFACE, WAVELENGTH IN METERS: 20.0

Figure 4.3 Listing of data file used to determine target (object plane) parameters.

The left hand image in Figure 4.4 shows the impulse response of the radar to a point target located at 150 m range. Single element SNR for this image was set at +15 dB. The right hand image shows the relative radar cross section distribution in the object plane. The average clutter level in the image is greater than 25 dB below the target level.

B. Prediction of Signal–to–Noise Ratio

Prediction of SNR requires knowledge of radar parameters such as antenna gain, power transmitted and noise figure, as well as models for target radar cross section as a function of parameters such as incidence angle and surface conditions. Program FSIMSNR written in FORTRAN, computes SNR based on the pulse–width limited radar range equation (2.1) and a zeroth order model of ocean surface scattering [25] which accounts for ocean wind speed and direction.

Figure 4.5 is a listing of the data file for program FSIMSNR. Typical values for the radar and ocean wind conditions are shown. This program generates two data files, SNR.DAT and RCS.DAT. SNR.DAT is a table of computed SNR as a function of range; RCS.DAT is a table of radar cross sections versus incidence angle. Both of these files are used by program FARSIM to model scattering from the ocean surface using a simple tilt modulation assumption. Ocean surface images generated using this information are given in Chapter V.

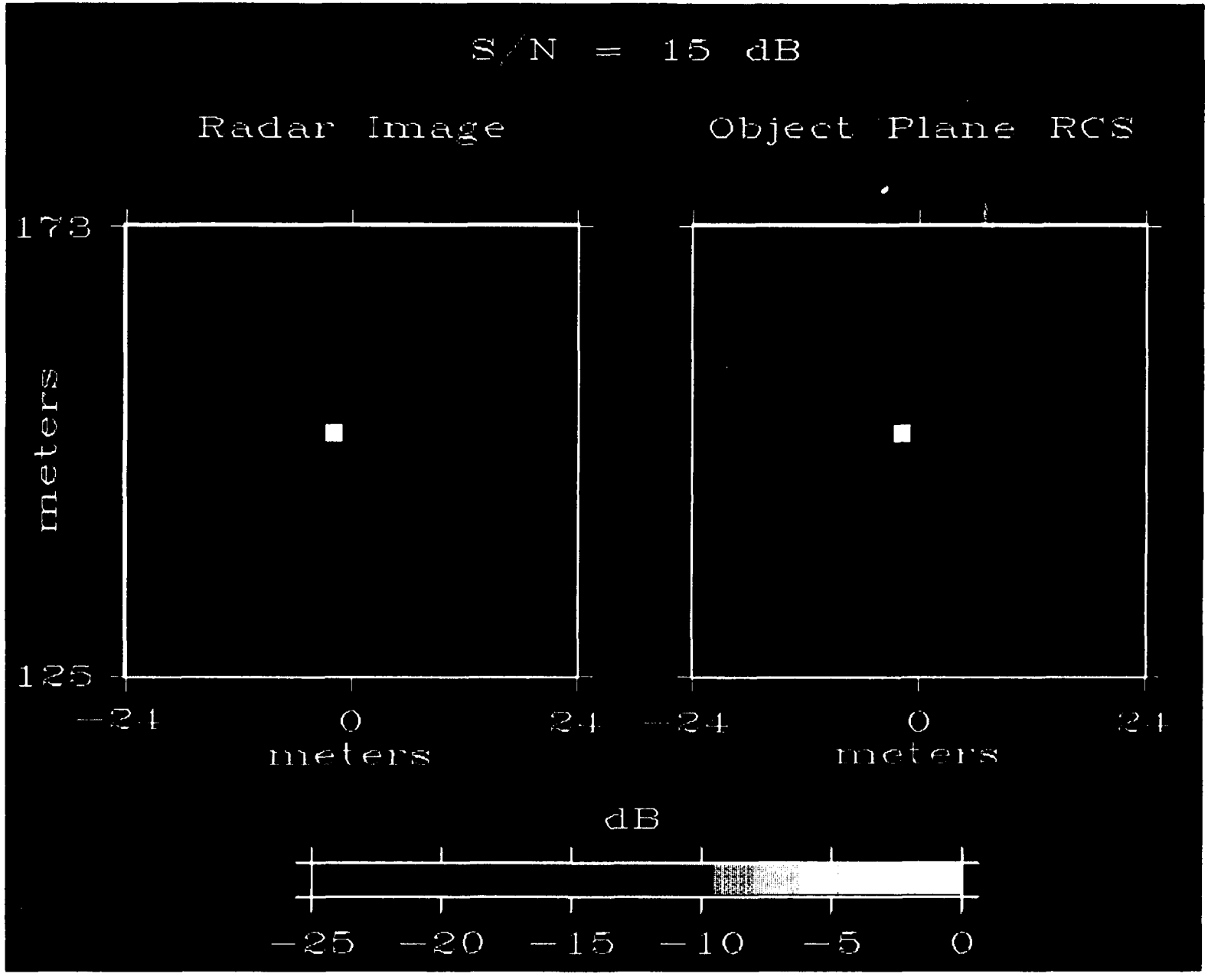

Figure 4.4 Impulse response of target as measured by radar with SNR = +15 dB (left); target amplitude distribution (right).

THIS DATA FILE CONTAINS INFORMATION ON THE SYSTEM CHARACTERISTICS OF THE FOCUSED ARRAY RADAR FOR SNR COMPUTATION

TRANSMIT POWER, PT, IN WATTS: 20.0

FULL ANTENNA GAIN, G IN DB: 36.3

FREQUENCY IN GHz, FREQ: 10.2

AZIMUTH BEAMWIDTH OF FULL ARRAY, AZ_BEAMWIDTH, IN DEGREES: .32

PULSE WIDTH, IN NANO_SECONDS, TAU_NS: 12.0

NOISE BANDWIDTH IN MHz, BANDWIDTH_MHZ: 100.0

RECEIVER NOISE FIGURE, NF, IN DB: 4.0

TWO-WAY SYSTEM LOSSES, L_SYS_DB, IN DB: 19.0

HEIGHT OF ARRAY, ZARRAY, IN METERS (CHESAPEAKE LIGHT TOWER IS 28 M): 28.

WIND SPEED, V, IN M/S: 7.5

WIND DIRECTION INDEX, IWIND, 0 FOR UPWIND, 1 CROSS-WIND, 2 DOWN-WIND,3= U/C: 3

Figure 4.5 Listing of data file used to compute signal–to–noise ratio.

Chapter V

Applications

In this chapter we discuss several possible applications of the focused array radar, including both imaging and nonimaging scenarios. Both scenarios take advantage of the large physical aperture of the antenna, which provides fine azimuthal resolution with a wide angle (20°) field of view. Imaging applications contrast with nonimaging in that images require many pixels in two dimensions (azimuth and range) while the nonimaging applications can be limited to one dimension (azimuth) with a single range sample. Imaging applications include imaging ocean waves, detection of ship wakes, studying degradation in SAR images due to finite velocity of the antenna, and making a motion picture of ocean radar cross section. There are other useful applications which do not require full images. High resolution studies of radar cross section statistics of a relatively small area of the ocean surface is one possible nonimaging application. Several applications of the focused array radar are discussed below.

A. Ocean Surface Imaging

The primary advantage of the focused array radar described in this report over convention radars is its ability to generate an image of a surface without physical or electronic beam scanning. Images generated of the ocean surface with resolution on the order of 1m × 1m will exceed the resolution normally obtainable with synthetic aperture radars, and will be generated in less than 1 mS, thus avoiding image distortion in SAR images due to Doppler histories of the various waves within the image. Using the software described in Chapter IV, we have generated images of a highly idealized ocean surface.

Figure 5.1 compares an image of a tilt modulated ocean surface made with the radar to the actual radar cross-section image generated by the computer. The image is 48 m wide and 48 m long, beginning 125 m from the base of the tower. Note that the radar image accurately reproduces the dominant wave length of 20 m. The wave amplitude was set at 1 m for this example. In creating the images 25 independent samples of a Rayleigh fading process were averaged. If we assume a decorrelation time of 10 mS for the ocean surface, this amounts to averaging for 0.25 seconds. For comparison, a single realization of a tilt modulated surface is shown in Figure 5.2 for a 1 m wave height. It is apparent that the speckle inherent in a single realization of the surface greatly reduces the interpretability of the image. Spatial averaging of adjacent pixels may also be used to reduce speckle if one wishes to limit the degree of time averaging employed.

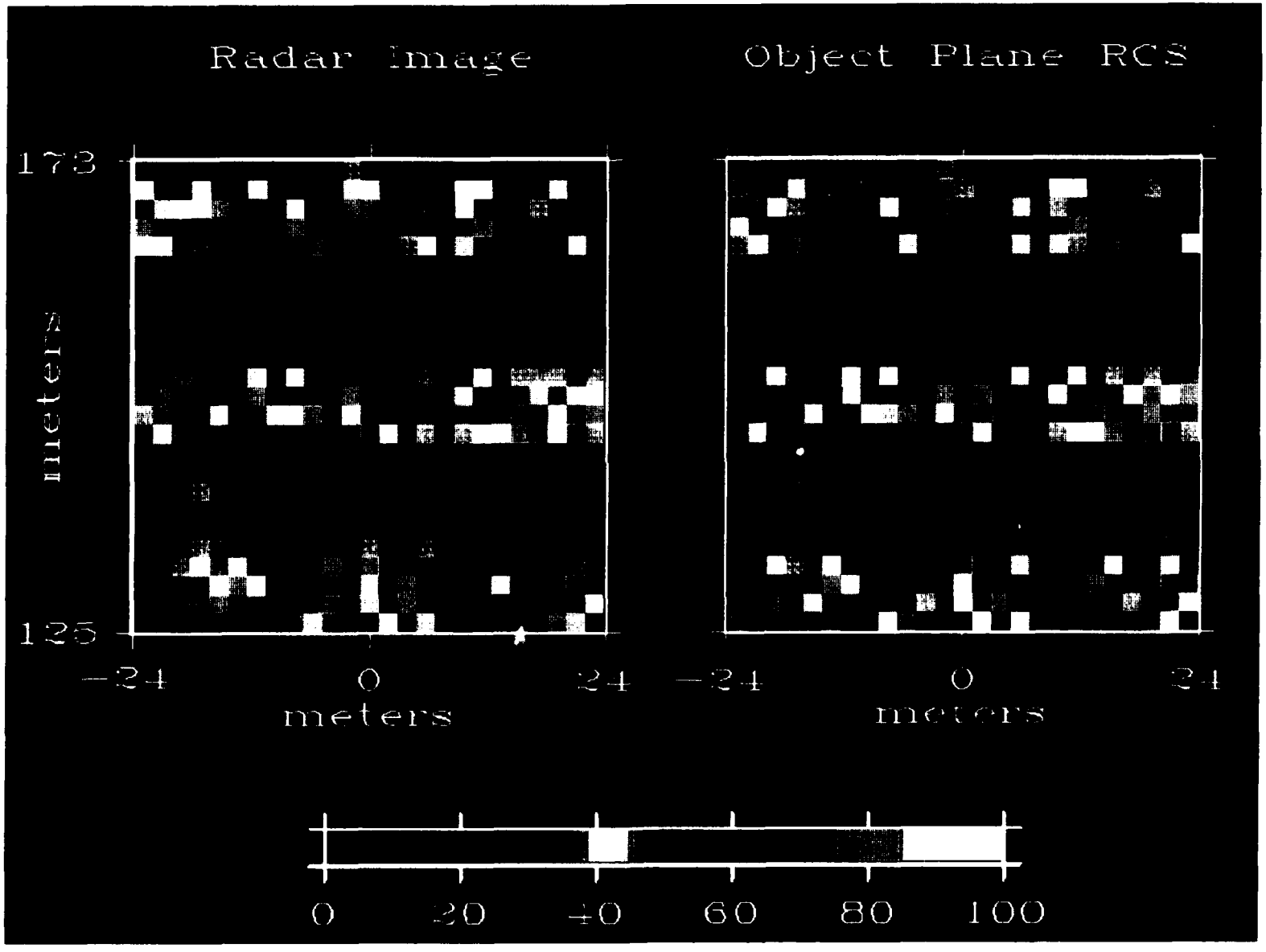

Figure 5.1 Image of tilt modulated ocean surface as measured by radar (left); distribution of ocean surface scattering amplitudes (right), (average of 25 images to reduce speckle).

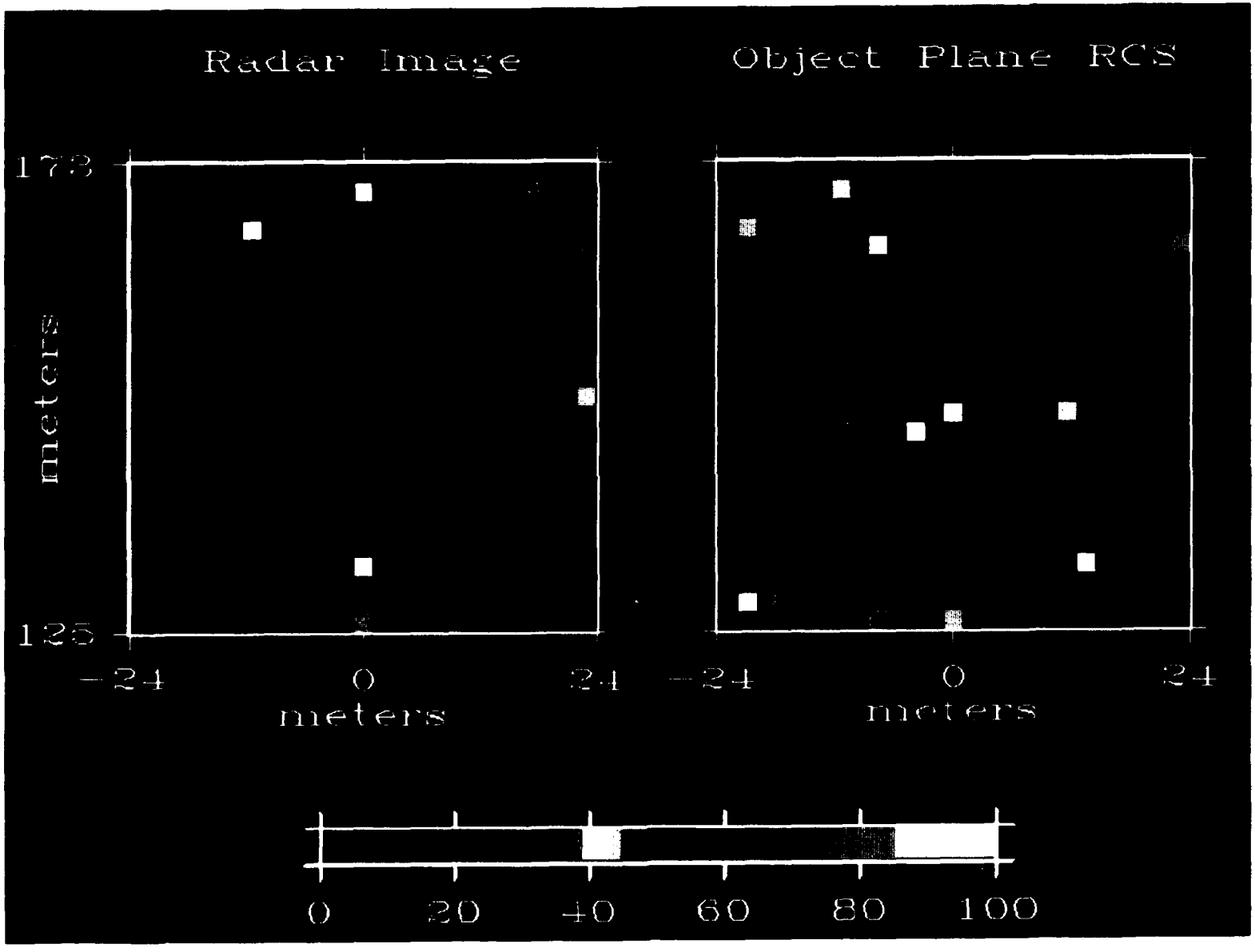

Figure 5.2 Single realization of tilt modulated ocean surface as measured by radar (left); distribution of ocean surface scattering amplitudes (right), (single iteration showing reduced interpretability due to speckle).

B. Time Delay Processing of Images

One useful application of the focused array radar will be to study degradation in ocean surface images as a function of synthetic velocity. In a SAR, a real aperture antenna, usually a few m in length, is flown along a straight path at a constant velocity. If the motion of the antenna is carefully controlled or monitored, and the surface is known to remain still, then the resolution of the final image is approximately $D_{\text{array}}/2$, where D_{array} is the length of the real aperture. However, resolution will degrade if the surface being imaged is moving in a unknown manner. Image resolution may be cast in terms of the range to velocity ratio, R/v [28]. For most SAR applications, R/v is of the order of 10–200. In the case of the focused array radar, the full 5.2 m aperture may be sampled in 719 μS, thus a synthetic velocity of 5.2/.000719=7230 m·s^{-1} is achieved. For a typical range of 200 m, this results in an R/v ratio of .0277, which results in negligible resolution degradation (see Appendix B). However, it is possible to generate any arbitrary value of R/v by varying the delay between measurements of adjacent elements in the array. More useful, though, would be to gather a multiplicity of images using a rapid scan rate, each having R/v =.0277, then processing the first element of the first image, along with the second element of the second image, and so forth, as shown in Figure 5.3. In this way, images generated with several synthesized R/v ratios may be generated. One interesting application would be to combine measurements using the focused array radar with over flights using a SAR. The focused array radar data may be processed using an R/v ratio similar to the SARs, as well as with low R/v values to extract the underlying radar cross section history, which has been lost in the SAR's imaging process.

C. Nonimaging Applications

To this point in the report we have discussed the radar in terms of ocean surface imaging. While this capability may have several interesting applications, such as imaging ocean waves, detection of ship wakes, or making a motion picture of ocean radar cross section, there are other useful applications which do not require full images.

1. *Radar Cross Section Statistics Versus Pixel Size*

The dependence of ocean radar cross section statistics on pixel size may be conveniently studied with the focused array radar since the radar footprint may be controlled in software after data has been collected. Thus, while studies using conventional radars would require either several radars or several separate antennas, the focused array concept allows the statistical dependence on footprint size to be determined using a single data set. Thus, one is assured that the ocean surface conditions were identical for all generated distributions. The pixel size may be degraded in azimuth by processing the image with a

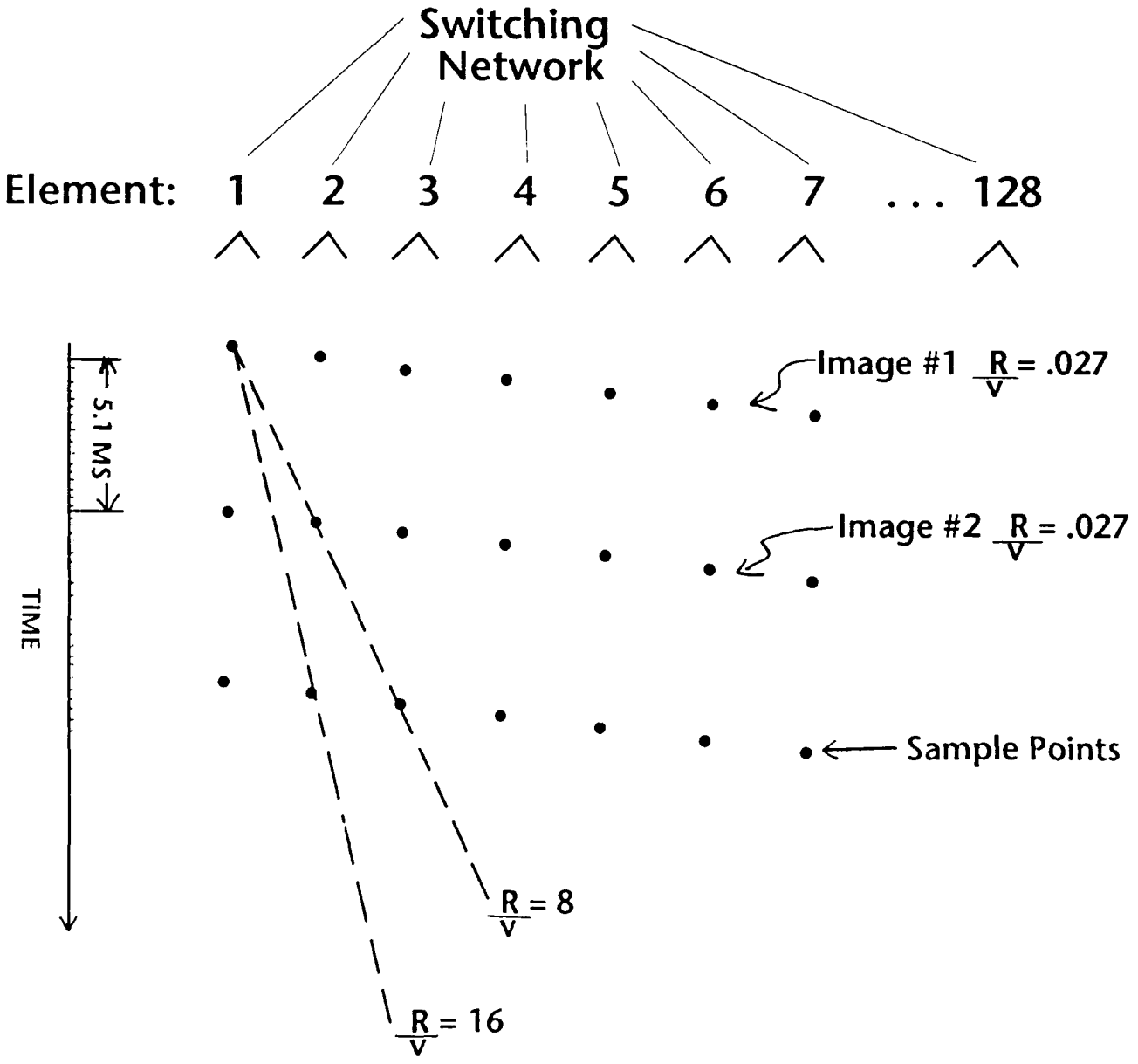

Figure 5.3 Time delay processing.

subsection of the array as shown in Figure 5.4. Indeed, several subsections may be used to process each degraded pixel, each subsection giving an independent look at the same fading process at one "instant" in time (an "instant" having 719 μS duration).

2. *Near Grazing Studies*

One application of such a technique, of current interest to the Navy, is to study ocean radar cross section statistics near grazing. While such studies would be impractical from a height of 20–30 m (the range would be too great for high SNR), the radar may be lowered to a height of 5 m, which would allow near grazing (87–89°) studies between 100–300 m range. Figure 5.5 shows the geometry of the grazing measurements along with a table of pixel size versus incidence angle. Note that the pixel size is less than 2 m$\times$2 m in all cases.

D. Other Applications

There are several other obvious applications of the focused array radar system which are worth mentioning. Due to the coherent nature of the radar it is possible to create radial velocity maps of the ocean surface, provided the sampling rate exceeds the Nyquist sampling criteria for Doppler shifted signals. While radial velocity images may not provide complete information, it is conceivable that two such instruments could observe the same footprint, thereby providing complete surface velocity information.

Another possible application of the radar would be to rapidly scan the ocean surface in azimuth through a 360° sweep. Such a scheme would require a tower providing an unobstructed view of the ocean surface which is not possible from the Chesapeake tower, but could be achieved from other platforms, such as a stable buoy or ship. Although at first glance it appears that such a scan mode could be achieved with a conventional scanning antenna, it must be remembered that conventional arrays are focused at infinity, and therefore could never achieve similar resolutions at comparable ranges.

E. Commercial Spinoffs

During the course of the Phase I investigation, we explored the possibility of applying focused array radars techniques to other areas, separate from ocean remote sensing. The ability of such a radar to generate high resolution images suggests its application to problems of night/ low–visibility vision problems. For example, such a radar could be used to as a landing aid to pilots approaching runways under low visiblity conditions. While the X–band array would be prohibitively large, the design could be scaled in frequency by a factor of 5 (50 GHz), where a 1.05 m long array would give similar resolutions. Such an imaging system would require a real time digital signal processor running at 50–100 MFLOPS, which is within the realm of possibility with current technology. It is also possible that such a system could aid in shipboard navigation through narrow channels under adverse weather conditions with more modest processing and antenna constraints.

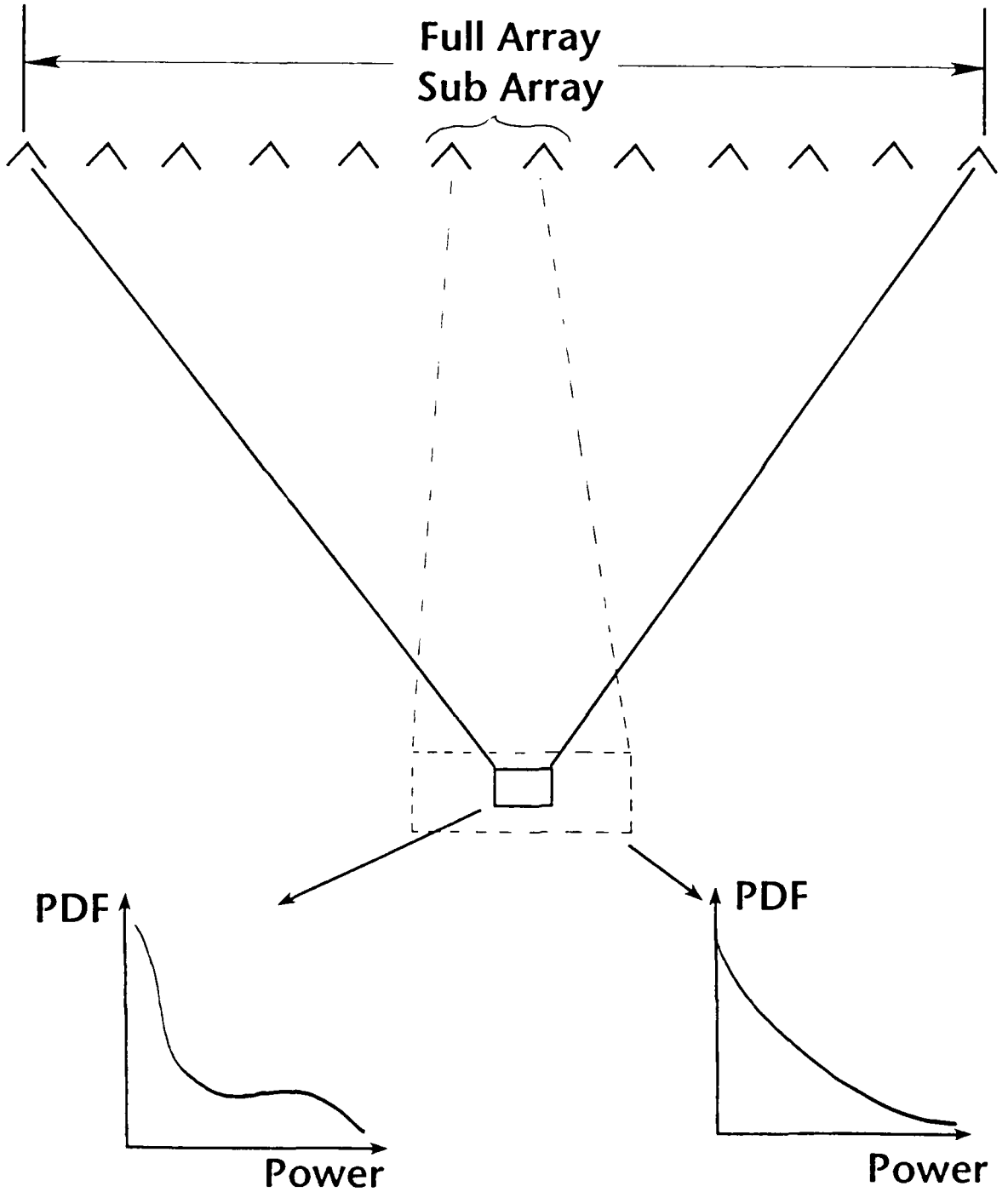

Figure 5.4 Measuring ocean surface reflectance statistics as a function of pixel size.

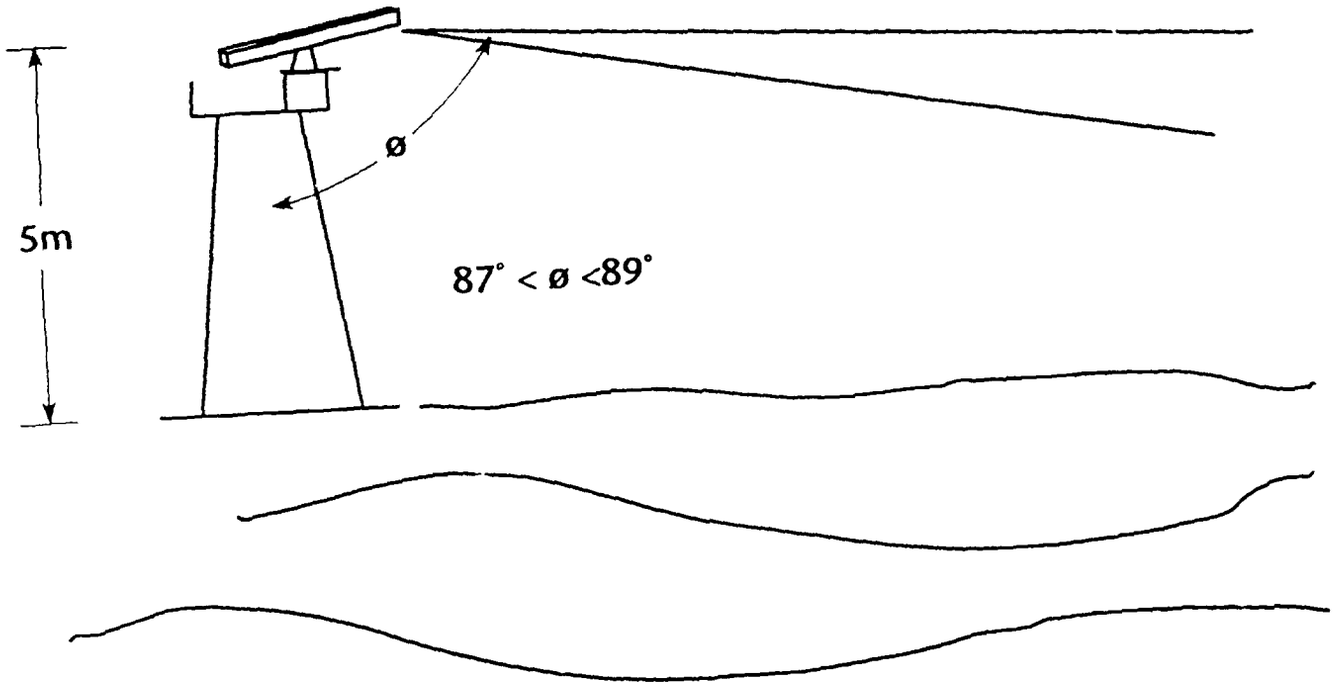

ø	Resolution	
87°	.5 x 1 (m)	(No Chirp)
88°	.8 x 1.8	(Chirp)
89°	1.6 x 1.8	(Chirp)

Figure 5.5 Geometry of near grazing measurements.

References

1. W. L. Jones, L. C. Schroeder, and J. L. Mitchell, "Aircraft Measurement of the Microwave Scattering Signature of the Ocean," IEEE J. Oceanic Eng., Vol. OE-2, p. 52, 1977.
2. R. K. Moore and A. K. Fung, "Radar Determination of Winds at Sea," Proc. IEEE, Vol. 67, pp. 1504-1521, 1979.
3. M. A. Donelan and W. J. Pierson, "Radar Scattering and Equilibrium Ranges in Wind-Generated Waves with Applications to Scatterometry," J. Geophys. Res., Vol. 92 (C5), pp. 4971-5029, 1987.
4. L. C. Schroeder, D. H. Boggs, G. J. Dome, I. M. Halberstam, W. L. Jones, W. J. Pierson and F. J. Wentz, "The Relationship Between Wind Vector and Normalized Radar Cross Section Used to Derive SEASAT-A Satellite Scatterometer Winds," J. Geophys. Res. 87, pp. 3318-3336, 1981.
5. T. R. Larson, L. I. Moskowitz and J. W. Wright, "A Note on SAR Imagery of the Ocean," IEEE Trans. Antennas and Propagation, AP-24, pp. 393-394, 1976.
6. C. E. Elachi and W. E. Brown, "Models of Radar Imaging of the Ocean Surface Waves," IEEE Trans. Antennas and Propagation, AP-25, pp. 84-95, 1977.
7. R. A. Shuchman, "Processing Synthetic Aperture Radar Data of Ocean Waves," *Oceanographic from Space*, ed. by J. F. R. Gower, pp. 477-496, Plenum, New York, 1981.
8. C. T. Swift and L. R. Wilson, "Synthetic Aperture Radar Imaging of Moving Ocean Waves," IEEE Trans. Antennas and Propagation, AP-27, pp. 725-729, 1979.
9. R. K. Raney, "Wave Orbital Velocity, Fade, and SAR Response to Azimuth Waves," IEEE J. Oceanic Eng., OE-6, pp. 4, 1981.
10. G. R. Valenzuela, "An Asymptotic Formulation for SAR Images of the Dynamical Ocean Surface," Radio Science, Vol. 15, pp. 105-114, 1980.
11. W. D. Alpers, D. B. Ross and C. L. Rufenach, "On the Detectability of Ocean Surface Waves by Real and Synthetic Aperture Radar," J. Geophys. Res., Vol. 86, pp. 6481-6498, 1981.
12. R. A. Shuchman, et al., "Analysis of MARSEN X-band SAR Ocean Wave Data," J. Geophys. Res., VOl. 88, pp.9757-9768, 1983.
13. K. Ouchi, "Effect of Defocussing on the Images of Ocean Waves," *Satellite Microwave Remote Sensing*, ed. by T. D. Allan, pp. 209-222, Ellis Horwood, Chichester, England, 1983.
14. W. J. Plant and W. C. Keller, "The Two-Scale Radar Wave Probe and SAR Imagery of the Ocean," J. Geophys. Res., Vol. 88, pp. 9776-9784, 1983.

15. K. Hasselmann, et al., "Theory of Synthetic Aperture Radar Ocean Imaging: A MARSEN View," J. Geophys. Res., Vol. 90 (C3), pp. 4659–4686, 1985.
16. O. H. Shemdin and L. D. McCormick, "SAXON 88/90 Science Plan", Ocean Research and Engineering, Pasadena, CA, March, 1988, p. 15.
17. F. E. Nathanson, *Radar Design Principles*, McGraw–Hill, New York, 1969, pp. 63–67.
18. M. I. Skolnik, ed. *Radar Handbook*, McGraw–Hill, New York, 1990, pp. 2.10–2.63.
19. L. V. Blake, Radar Range–Performance Analysis, D.C. Heath and Company (Lexington Books), Lexington, MA, 1980. 2d ed., Artech House, Norwood, MA, 1986.
20. W. E. Scharfman and G. August, "Pattern Measurements of Phased–Arrayed Antennas by Focusing into the Near Zone," in *Phased Array Antennas*, A.A. Oliner and G.H. Knittel, eds. Artech House, Dedham, MA. pp. 344–350.
21. J. W. Sherman, "Properties of focused Apertures in the Fresnel Region," IRE Trans. Ant. Prop., July, 1962, pp. 399–408.
22. D. L. Mensa, *High Resolution Radar Imaging*, Artech House, Norwood, MA, 1981.
23. J. D. Kraus, *Antennas*, McGraw–Hill, 1950, pp. 66–69.
24. F. T. Ulaby, R. K. Moore, and A. K. Fung, *Microwave Remote Sensing, Active and Passive, Vol. II*, Artech House, Norwood, MA, 1982, pp. 644–647.
25. E. P. W. Attema, A. E. Long and A. C. Gray, "Results of the ESA Airborne C–Band Scatterometer Campaigns, ESTEC, Noordwijk, Holland, 1985.
26. M. W. Long, *Radar Reflectivity of Land and Sea*, Artech House, Norwood MA, 1983, pp. 267–275.
27. F. T. Ulaby, R. K. Moore, A. K. Fung, *Microwave Remote Sensing, Active and Passive, Vol. II*, Artech House, Norwood, MA, 1982, pp. 682–686.
28. C. L. Rufenach and W. R. Alpers, "Imaging Ocean Waves by Synthetic Aperture Radars with Long Integration Times," IEEE Trans. Ant. and Prop., vol. AP–29, No. 3, May, 1981, pp. 422–428.

Appendix A

Azimuthal Resolution Degradation Due to Ocean Surface Motion in Focused Arrays and SARs

During the meeting at WHOI (5-18-90), a discussion of the ability of the focused array to simulate the R/v ratios typical of airborne/spaceborne SARs arose. In particular, we questioned the ability of the focused array to yield the same azimuthal resolution, ρ, as the SAR. Neglecting the effects of orbital motion, the azimuthal resolution of a SAR imaging a time-varying target is given by [1,2]

$$\rho = \frac{N\lambda R}{2v}\left(\frac{1}{T^2} + \frac{1}{N^2\tau^2}\right)^{1/2} \tag{1}$$

where

N is the number of looks

$\frac{R}{v}$ is the range to velocity ratio, a fixed quantity in most SAR applications,

λ is the radar wavelength,

T is the time used to form an image (integration time), and

τ is the decorrelation time of the pixel being imaged.

Letting $N = 1$ (throughout this discussion) for $T \ll \tau$, ρ reduces to $\frac{\lambda R}{2vT}$ which for $vT = L_{array}$ can be shown to reduce to the conventional SAR resolution $\rho = D/2$ where D is the width of the physical antenna in the along track direction. For $T \gg \tau$, ρ reduces to $\frac{\lambda R}{2v\tau}$ where $v\tau$ may be thought of as an effective aperture length $L_{effective}$. Thus, for rapidly decorrelating targets, $L_{effective}$ is short and the SAR resolution will degrade substantially from the optimal $D/2$ value.

It is possible to use a sequentially sampled focused array of fixed length, L_f, to simulate SARs having various R/v ratios, although the focused array integration time, T_f, is coupled to v through

$$v = L_f/T_f \; . \tag{2}$$

It is informative to recast equation (1) in terms of L_f and T_f, replacing the somewhat artificial quantity of velocity. Thus substituting (2) into (1) yields

$$\rho = \frac{\lambda R}{2L_f}\left(1 + \frac{T_f^2}{\tau^2}\right)^{1/2} \tag{3}$$

For $T_f \ll \tau$, ρ reduced to $\frac{\lambda R}{2L_f}$ which is consistent with the result I presented at the WHOI meeting. (I had $\frac{\lambda R}{L_f}$ which assumed a $\cos^{1.8}$ taper.)

For $T_f \gg \tau$, ρ reduces to $\frac{\lambda R}{2L_f}\left(\frac{T_f}{\tau}\right)$ which increases linearly with T_f. During our discussion at WHOI, we interpreted (3) as differing significantly from (1) for large integration times. Shown graphically in Figure A.1, (1) is seen to converge to the limit $2R/v\tau$ for large T, while (3) increases as T_f for large T_f. Upon reflection, this should have struck us as unusual considering equation (1) and (3) are equivalent, provided (2) holds. This

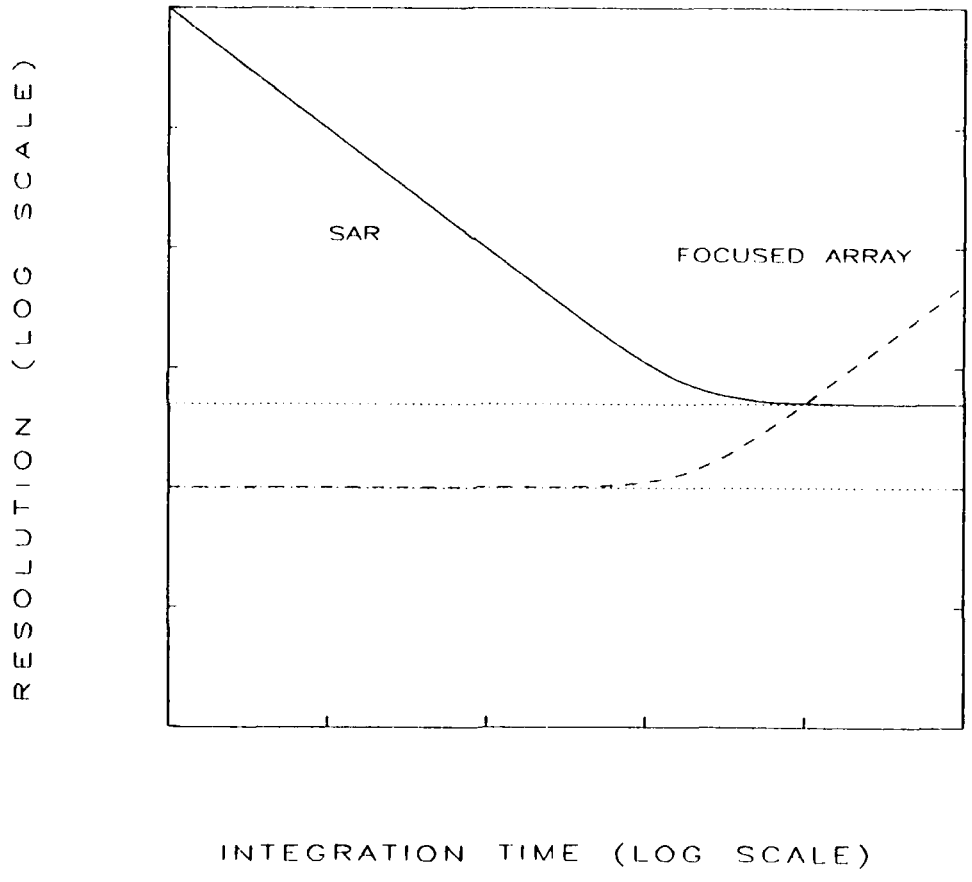

Figure A.1 Comparison of SAR (——) and focused array (- - - -) resolutions as a function of integration time. Long integration time limit for SAR $= \lambda R/2v\tau$. Short integration time limit for focused array $= \lambda R/2L_f$.

confusion results from the fact that (1) plotted in Figure A.1 assures a fixed R/v while (3) has

$$R/v = \frac{RT_f}{L_f} \ . \tag{4}$$

A more informative way to compare (1) and (3) is to plot a family of curves for (1) at various R/v. In the table below, T_f is given for various values of R/v using (4), assuming $L_f = 10$ meters and $R = 1000$ meters.

R/v	T_f
.1	.001 s
1.0	.01 s
10.0	.10 s
100	1.0 s

In Figure A.2, a plot of (1) with R/v as a parameter, along with (3), shows that (1) and (3) are indeed equivalent when T_f is chosen to match R/v. In this plot, I have assumed $D = 100\ \lambda$, ($\beta = .01$ radians) and $\tau = .1$ s. It is evident that a focused array of fixed length may be used to study the effect of varying R/v and will give the same result as an airborne SAR.

Equation (1) becomes more complicated if the effects of orbital acceleration are included. Rufenach and Alpers [2] give the complete expression as

$$\rho = \frac{N\lambda R}{2v\tau}\left[1 + \frac{1}{N^2}\left\{\left(\frac{T}{\tau_s}\right)^2 + \left(\frac{\pi}{\lambda}T^2\hat{a}_r(x_0)\right)^2\right\}\right]^{1/2} \tag{5}$$

where

$\hat{a}_r(x_0)$ = the orbital acceleration of the ocean waves

$\hat{a}_r(x_0) = \hat{\zeta}_0\hat{\omega}^2 g(\theta,\phi)\cos(\hat{k}_x x_0 + \delta)$

and

$g(\theta,\phi)$ = geometric factor (=1 for azimuthally traveling waves)

$\hat{\zeta}_0$ = ocean wave amplitude

$\hat{\omega}$ = ocean wave angular frequency

k_x = ocean wave number

x_0 = azimuthal position

δ = fixed phase term

For typical ocean and SAR conditions, the following inequality holds:

$$\left(\frac{T}{\tau_s}\right)^2 \ll \left(\frac{\pi}{\lambda}\hat{a}_r T^2\right)^2 \tag{6}$$

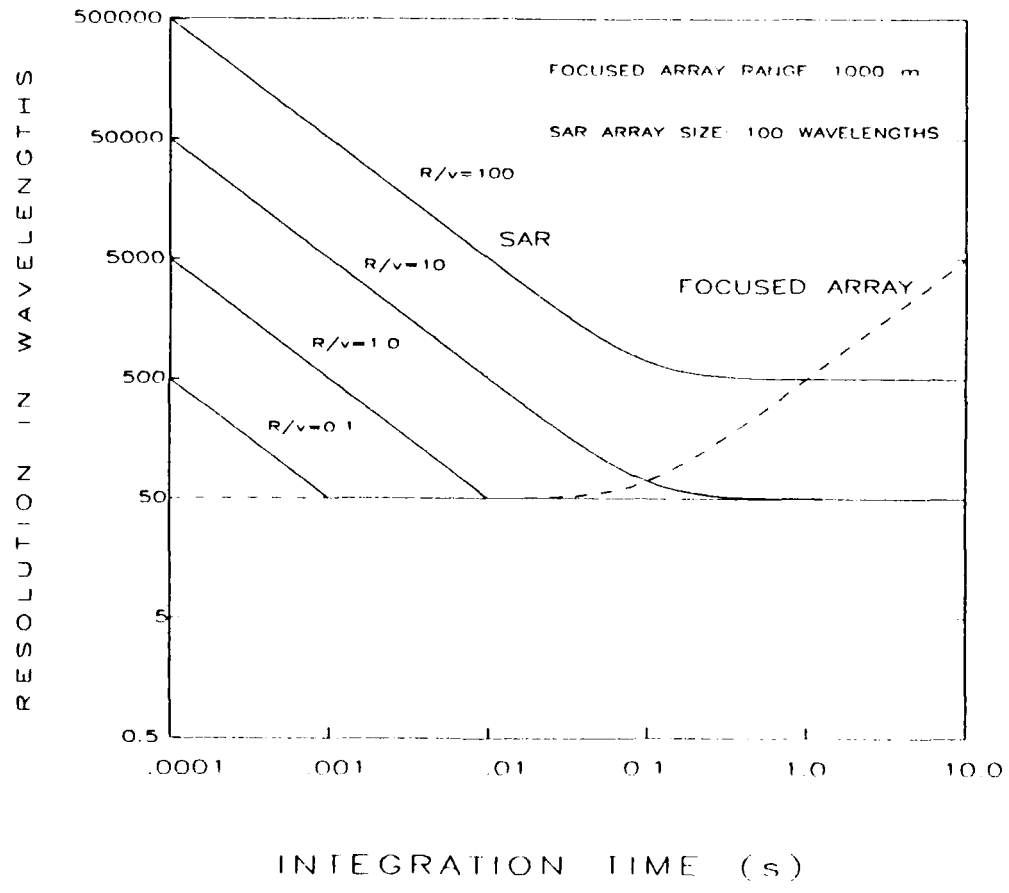

Figure A.2 Comparison of SAR (——) and focused array (- - - -) resolution for specific values of R/v. Resolutions for SAR and focused array are equal when (2) is satisfied.

Thus, the effects of orbital motion most likely will dominate image degradation. As before, there is no fundamental difference between the real SAR and the focused array, provided the resolution does not degrade beyond the maximum achievable by the focused array. This maximum value will occur when ρ is equal to the azimuthal swath width, i.e., $\rho_{max} \cong \frac{\lambda R}{D_{eff}}$ where D_{eff} is the effective azimuthal width of the individual radiating element in the focused array (approximately 2λ in the proposed design). Equating (5) to ρ_{max} and solving for $(R/v)_{max}$ and assuming the term due to orbital motion dominates, gives

$$\left(\frac{R}{v}\right)_{max} = R\sqrt{\frac{2\lambda}{D_{eff}L_f\pi\hat{a}_r}} \tag{7}$$

For $R = 100$ m, $D_{eff} = .10$ m, $\lambda = .05$ m, ocean wave height = 1 meter and wave frequency $= .4\ s^{-1}$, $\left(\frac{R}{v}\right)_{max} = 44$, which is lower than spaceborne SARs ($\frac{R}{v} \cong 120$) but is in the range of typical values for airborne SARs. It should be noted that this analysis is based on a monochromatic sea spectra, and is thus highly idealized. Thus (7) should be used to give a rough estimate of $(\frac{R}{v})_{max}$.

Although the focused array can be sampled to yield the same azimuthal resolution as the SAR, it is likely that the images generated by the focused array will not be identical to those produced by a SAR with the same azimuth resolution. For a true SAR, biases in the Doppler history of azimuthally traveling waves due to their along-track motion will cause shifts in their apparent position. This will cause waves which are physically at one location to shift over several pixel widths in the image. The limited swath width of the focused array will prevent it from observing scattered power from waves falling outside the swath, thus such waves will not affect the image formed within the swath, as would happen in the SAR. Thus, it is likely that the focused array will not yield the same image as a SAR having the same resolution.

[1] Raney, R. K., "SAR Response to Partially Coherent Waves," IEEE Trans. Antennas and Prop., Vol. AP-28, No. 6, November 1980, pp. 777-787 (Eq. 39).

[2] Rufenach, C. L., Alpers, W. R., "Imaging Ocean Waves by Synthetic Aperture Radars with Long Integration Times," AP-29, No. 3, May 1981, pp. 422-428.